TEMPLATE ASSISTED MANUFACTURING OF LOW-TEMPERATURE COPPER-BASED NANO SOLDER

by

CARLOS J. MORALES DEL VALLE

A thesis submitted in partial fulfillment of the requirements for the degree of

MASTER OF SCIENCE
in
MECHANICAL ENGINEERING

UNIVERSITY OF PUERTO RICO
MAYAGÜEZ CAMPUS
2012

Approved by

_____   _____
Ricky Valentín, Ph D.   Date
President, Graduate Committee

_____   _____
David Dooner, Ph D.   Date
Member, Graduate Committee

_____   _____
Pedro Resto, Ph D.   Date
Member, Graduate Committee

_____   _____
Gustavo Gutierrez, Ph D.   Date
Chairperson of the Department

_____   _____
Moisés Orengo Ph D.   Date
Representative of Graduate Studies

ABSTRACT

As a response to new legislation and calls to lead-free technologies, a method is proposed to manufacture nano-copper by means of electroless copper plating on nanofibers templates. Polyacrylonitrile (PAN) nanofibers were prepared by electrospinning solutions of said polymer and dimethylformamide. The fibers were cleaned, etched and activated using chemical solutions for subsequent copper deposition. The coating solution was found to properly reduce copper when maintained at a pH of 11-12.

SEM and optical characterization revealed copper deposited on the fibers making a 250 nm layer around the 500 nm nanofibers. A melting point range for the manufactured nano-copper was determined by heating samples at different temperatures in a high temperature oven. Results showed how first the copper on the nanofiber melts at around 600°C and complete melting of the copper occurs at 800°C. Once the melting temperature range was determined, samples were prepared for mechanical testing. Copper strips were soldered together with the nano-copper in the oven and tested on a tensile strength tester. Specimens failed at loads of 10-60 N, showing to have appropriate mechanical properties for solder applications.

RESUMEN

Como respuesta a la nueva legislación y las llamadas a tecnologías libres de plomo, se propone un método para la fabricación de nano-cobre por medio de deposición química de cobre y el uso de nanofibras como plantillas. Nanofibras de poliacrilonitrilo (PAN) fueron preparados por 'electrospinning' utilizando soluciones de dicho polímero y dimetilformamida. Las fibras fueron limpiadas, grabadas y activadas usando soluciones químicas para luego ser recubiertas con cobre. La solución de recubierta reducía el cobre apropiadamente al mantener el pH entre 11-12.

Caracterización óptica y en el SEM demostró que se formaba una capa de cobre con un espesor de 250 nm alrededor de las fibras de 500 nm. Un intervalo de punto de fusión para el manufacturado nano-cobre se determina mediante el calentamiento de las muestras a diferentes temperaturas en un horno de alta temperatura. La experimentación mostró cómo primero el cobre en la nanofibra funde a alrededor de 600 ° C y de fusión completa del cobre se produce a 800 ° C. Una vez que el rango de temperatura de fusión es determinado, las muestras se prepararon para el ensayo mecánico. Tiras de cobre fueron soldadas entre sí con el nano-cobre en el horno y probado en un probador de esfuerzo en tensión. Las muestras aguantaron cargas de 10 a 60 N, lo cual muestra propiedades mecánicas apropiadas para aplicaciones en soldadura.

To my family and friends, for their unconditional support and love throughout
my life and professional growth.

ACKNOWLEDGEMENTS

TABLE OF CONTENTS

LIST OF TABLES

LIST OF FIGURES

CHAPTER 1: INTRODUCTION

Many social and environmental reasons drive to the implementation of lead-free technologies. One of these reasons, of course, is lead being a poisonous metal that is capable of causing damage to every organ in the body, with the most harm being caused to the brain, nervous system, blood, and kidneys. Thus, proposed and enacted legislation in the form of international and national laws and environmental regulations require that solder alloys for electronic components and printed wiring board interconnections be lead-free.

On January 27, 2003, the European Parliament and the Council of the European Union passed a pair of directives aimed at minimizing the risks and impacts that the production, use, treatment, and disposal of waste electrical and electronic equipment have on human health and the environment. Directive 2002/95/EC on the restriction of the use of certain hazardous substances in electrical and electronic equipment (RoHS) and identifies lead as a material not allowed in electrical and electronic equipment to be put on the market after July 1, 2006. Other hazardous materials the directive restricts include are mercury, cadmium, hexavalent chromium, polybrominated biphenyls, and polybrominated diphenyls ethers.

The initial efforts by various companies and academic institutions were focused on the identification of possible replacement lead-free alloys. This led to the growth of patents on lead-free alloy compositions and applications. Table 1.1 shows some of the lead free allows recently manufactured and their concerns.

Table 1.1: Alternative basis metals to lead and their alloys. [23]

Element	Typical Composition	Melting Point (°C)	Remarks
Pb	62Sn/36Pb/2Ag 63Sn/37Pb	179 183	Well-established alloys; low price.
Ag	96.5Sn/3.5Ag	221	Good thermal fatigue; fast Cu dissolution.
Cu	95.5Sn/4Ag/0.5Cu 95.5Sn/3.8Ag/0.7Cu 95Sn/4Ag/1Cu 99.3Sn/0.7Cu	216-219 217-219 216-219 227	Prelimiinary tests show good thermal fatigue properties at high temperatures; favourably priced.
Bi	58Bi/42Sn 90Sn/2Ag//7.5Bi/0.5Cu 91.8 Sn/3.4Ag/4.8Bi	138 198-212 200-216	Suitable for low temperature applications. Creation of low melt. Sn/Bi phase at 138°C. Fatigue at high temperature under evaluation.
Sb	95Sn/5Sb 65Sn/25Ag/10Sb 96.7Sn/2Ag/0.8Cu/0.5Sb	232-240 230-235 217-220	High melting point; toxicity concern. Creation of needle shaped Ag_3Sn phases. Similar properties as Sn/Ag/Cu.
In	52In/48Sn 97In/3Ag 77.2 Sn/20In/2.8Ag 86.4Sn/11In/2Ag/0.6Sb	118 143 189	Expensive; limited availability; indium tends to corrode in combination with humidity and is very soft.
Zn	91Sn/9Zn	199	Problem of oxidation. Strong dross formation.
Au	80Au/20Sn	280	Much too expensive.
Cd	67Sn/33Cd	170	Toxicity.

The leading candidate alloys are tin-rich, with silver, copper, bismuth, and antimony as one or more major alloying elements. From the manufacturing standpoint, the melting points (and hence reflow temperatures) and wetting characteristics of the solders are the key factors in proper solder interconnection.

Industry wide efforts focused on optimizing the selection of replacement lead-free alloys for specific applications, including component terminals and PCB assembly. Electronics system manufacturers investigated the effects of this change in terms of bill of materials, manufacturing infrastructure and process, system reliability and developed appropriate solutions. Advancements in lead-free technologies are providing manufacturers with opportunities to make process changes to incorporate different components and materials. Some have questioned the logic of eliminating lead in electronics, but initial consumer reaction to lead-free products has been positive, and early successes in marketing of these products suggest that informed consumers are choosing environmentally considerate products. [1]

1.1   Barriers to Lead-free Electronics

Lead-free technology replacing the current lead-based alloys should satisfy the following requirements to a reasonable extent [1]:

- low melting point

- comparable cost

- small pasty range (liquidus and solidus temperatures should be close)

- acceptable and consistent manufacturability (both at the component level and board level)

- acceptable wetting characteristics (to various surface finish on boards and components)

- acceptable physical properties: electrical and thermal conductivity

- acceptable mechanical properties (strength, ductility)

- compatibility with lead containing parts

- compatibility with fluxes

- low toxicity and recyclable

Reliability may in fact be of more concern than any potential manufacturing problems. As stated, the higher melting temperatures of the lead-free alloys require higher processing temperatures, which raise concern for effects on components and boards. However, the higher melting points translate into higher operating temperature ranges, which should enhance reliability for some products.

Complete assurance as to the long-term reliability of electronic products with lead-free assemblies will probably take some time to develop. However, some completed studies and others still underway have begun to address the reliability issue for new lead-free parts and products. Lead-free alloys must continue to be tested, as their reliability must be equal to or better than that of tin-lead. [1]

Straying away from the conventional lead-free alloys, the research described in the following pages will study a new approach in the manufacturing of lead-free solder. By studying the properties of nanomaterials, a method has been devised to manufacture a material that takes advantages of these properties with the potential of having lead-free solder applications.

1.2   Nano-solder Potential

Nanotechnology allows the manipulation of matter at the atomic level, enabling new approaches to material property enhancement. Solder materials containing nano-sized metals exploit the high surface area and high surface energy of nano-sized particles to lower the apparent melting point below the conventional melting point.

Pure metals, such as Sn, Pb, and Cu, are known to show significant melting temperature depression, with the amount of temperature depression increasing as the particle size decreases.

Researchers like S. L. Lai et al. [6] have demonstrated that nano-scale metal tin particles have a melting temperature that is more than 70°C below the melting point of bulk tin.

This particle-size-dependent melting point depression found in nanomaterials can therefore be beneficial as pure metal nano-particles can be used instead of alloys to achieve low melting solders. These nano-solders have the additional property of having their melting temperature return to normal once they melt and become bulk. This means that the nano-solder will have a low processing temperature to melt, but a high working temperature, meaning it will be able to work in high temperature applications.

1.3   Objectives

The primary objective of this investigation is to create a nano-solder by depositing copper on nanofibers by method of electroless plating. This process is very cost effective compared to most methods of producing nanomaterials and would therefore provide an efficient way to produce potential nano-solders. One major point of interest is to see whether the nano-size copper has a lower melting point temperature than bulk copper. Achieving this lower melting point temperature expectation would show that producing nanomaterials is a viable method of manufacturing nano-solders to replace existing solder containing lead.

This nano-solder will be tested to meet the following necessary requirements any lead-free solder should have when replacing current lead based solders: [1]

- Low melting point.
- Acceptable physical and mechanical properties.

CHAPTER 2: LITERATURE REVIEW

The following chapter is divided in two sections. The first presents the theory and current studies behind nanomaterial properties, particularly particle-size-dependent melting point depression. The second section focuses on methods of manufacturing nanomaterials, mainly with the assistance of templates.

2.1 Nanomaterial properties

One of the most unusual properties of nanometer-sized materials that is of interest for this research is particle-size-dependent melting point depression, which occurs when the particle size is of the order of nanometers. Generally speaking, the smaller the particle, the lower the melting point becomes. This is essential if lead free tin nano-solder is to be manufactured with the property of having a low melting point, preferably 183ºC or lower.

S. L. Lai et al. [6] measured the latent heat of fusion for Sn particles formed by evaporation on inert substrate with radii ranging from 5 to 50 nm using a scanning nanocalorimeter. Their results show a particle-size-dependent reduction of the latent heat, the amount of heat required for melting. This in turn causes a reduction in the melting point temperature as presented in Figure 2.1. From their results, we can see that to obtain a melting point of 183ºC or below, pure tin must have a particle diameter size of approximately 15 nm.
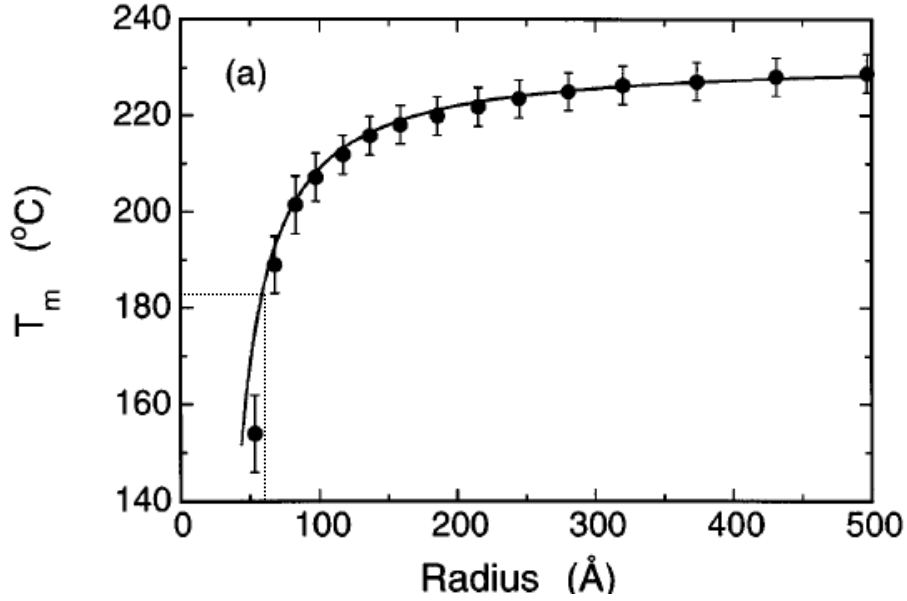
Figure 2.1: Size dependence of the melting points of Sn particles. [6]

In another paper, S.L. Lai et al. [16] investigated the melting point depression of Al clusters deposited onto a Si_3N_4 surface via thermal evaporation. They found that the melting point of these small Al clusters is significantly reduced, by as much as 140 °C as compared to the bulk values. J. Sun et al. [38] confirms melting point depression and decrease in heat fusion for aluminum nanoparticles. X.W. Wang et al. [29] demonstrated the same behavior in Zn nanowires prepared by electrodeposition in the holes of porous anodic alumina membranes.

M. Zhang et al. [15] studied the melting behavior of 0.1−10-nm-thick discontinuous indium films. The relationship between the nanostructure radius and the corresponding melting point and latent heat was deduced solely from experimental results ~i.e., with no assumed model. They show that the melting point of the indium nanostructures decreases as much as 110 K for particles with a radius of 2 nm. The melting point showed a linear decrease with curvature (1/r) within the experimental uncertainty.

Y. Shibuta et al. [42] studied the effect of particle size over melting point of iron nanoparticles. As expected, as the diameter of the nanoparticles decreased, so did the melting and nucleation temperature of the material. In their case, temperatures 300K lower than the regular melting point was achieved.

Another interesting property of nanoparticles concerning their melting point is superheating of embedded nanoparticles. K. Chattopadhayay et al. [40] highlights the importance of crystallographic shape in the melting transition. Embedded particles are expected to show superheating whereas, melting point depression rarely occurs. The nature of the matrix seems to also affect as the author explains how Pb particles embedded in a Cu matrix showed significant superheating over ones embedded in an Al matrix.

H.W. Sheng et al. [21] prepared two types of Pb-Al granular samples by using melt-spinning and ball-spinning techniques. Both had similar lead particle sizes but different interfaces with the aluminum depending on how it was prepared. It was found that the faceted Pb nanoparticles in the melt-spun sample could be superheated by about 11-40K, whereas the irregularly shaped Pb particles in the ball-milled sample melted about 13K below its equilibrium point. It is suggested that different interface structures, which cause variations in energy differences between solid-Pb-solid-Al and liquid-Pb- solid-Al interfaces, are responsible for the different melting behavior of Pb nanoparticles.

In a separate experiment, Sheng [39] studied the behavior of indium nanoparticles embedded in a porous alumina matrix prepared with the same techniques described before. Again, the epitaxially oriented particles in the matrix were superheated to about 38°C and randomly oriented particles melted below the equilibrium melting point by about 22°C. This suggests how

the melting point of these In nanoparticles can be manipulated to be either raised or depressed, depending on their orientation with the matrix.

The same team confirmed that embedded particles of In, Sn, Bi, Cd, and Pb would experience melting point depression as long as ball milling was used to prepare the samples. [41] This further confirms the importance of the nature of interface and orientation and the effect it has on the material's melting point.
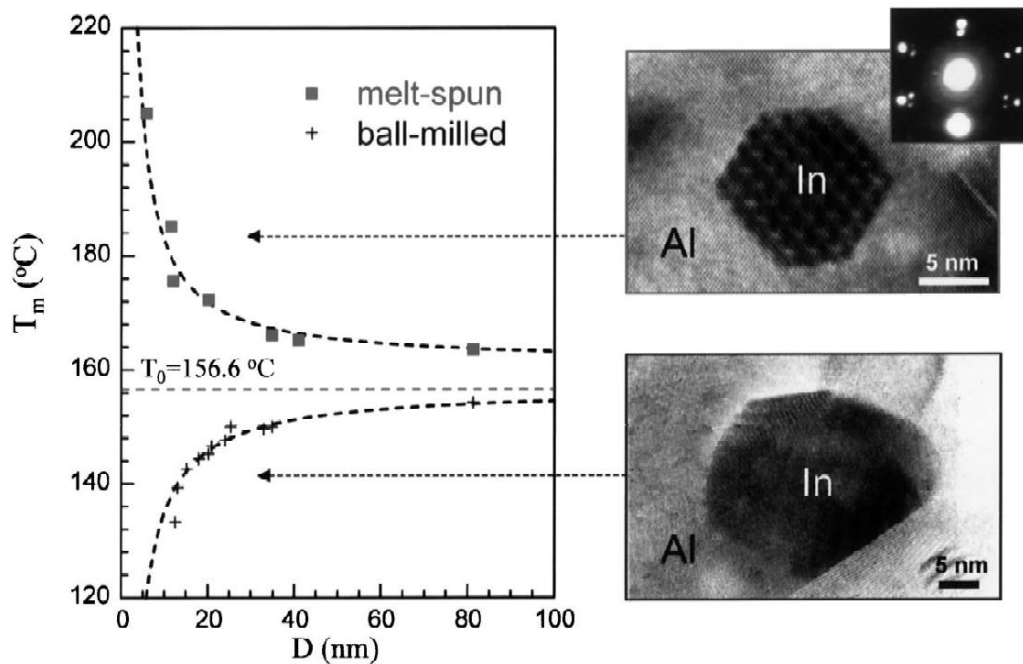
Figure 2.2: Melting point of Embedded In particles according to interface with matrix. [41]

K. Lu et al. [43] showed how the both methods used by the previous authors have inverse effects on the melting temperature of nanoparticles. As stated before, ball-milled particles exhibit depression while melt spun particles exhibit superheating.

R. Goswami et al. [22] also present an alternative to melting point depression other than size dependency. They report the formation of nanocomposites of Bi particles in a metallic glass

matrix and have shown that under a constrained solidification condition, they yield particles with multiple domains. They find an unusually large depression of the bulk melting points of the Bi particles which cannot be explained by the size effect and is clearly related to the phenomenon of the formation of crystallographically related multiple domains.

2.2   Template Assisted Synthesis of Nanomaterials

There have been several publications about different synthetic techniques that have successfully made nanowires of a large variety of materials. Many of these methods utilize templates as a way to control the growth and morphology of the nanowires. The following section summarizes the literature review done in the study of template assisted synthesis of nanomaterials.

2.2.1   Porous Alumina Templates

One of the most commonly used templates used for nanowire synthesis is the porous anodic alumina template. These are produced by anodizing pure Al films in various acids as shown in the figure below.
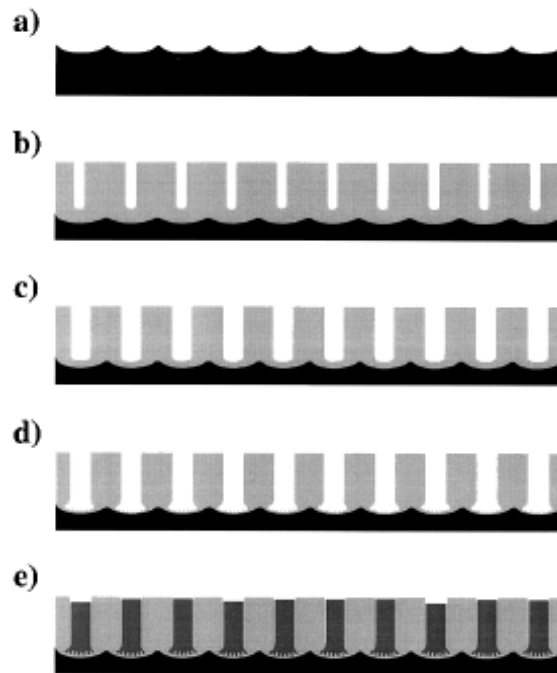
Figure 2.3: Manufacturing of Porous Alumina Templates [34]

First (a) the Al substrate is pre-structured by anodizing for a long period of time and removing the oxide. (b) A second anodization step produces a highly ordered alumina pore

structure. c) The barrier layer is thinned and the pores are widened by isotropic chemical etching. d) For further thinning of the barrier layer two current-limited anodization steps are used and pore formation occurs at the barrier layer. e) Eletrodeposition can be used to fill the pores with a desired metal. [34]

Mikhaylova et al. [4] successfully prepared a hexagonal arrayed porous anodic alumina membrane with which they later used to make Co and Fe nanowires by AC pulse electrodeposition. Their conclusions indicate that image analysis confirmed the formation of multicrystalline Co and Fe as nanotubes or nanowires depending on the electrodeposition conditions.

Shoso Shingubara [11] has studied how porous alumina nanohole arrays have been used to fabricate a variety of nanomaterials. These methods include: etching semiconductor substrate using a porous alumina film as a mask, pattern transfer using porous alumina as a template, deposition of functional materials in the form of porous alumina nanohole arrays by electroplating and sol–gel, and deposition of functional materials by chemical vapor deposition (CVD). The author also mentions that numerous studies have been conducted on the filling of conductive materials in porous alumina nanoholes by electroplating. Possible applications include coloring of the aluminum plate itself and magnetic recording media for a high-density magnetic disk. Sol–gel also provides an alternative synthesis route for nanomaterial fillings in porous alumina nanoholes. Hollow nanotubes comprising In_2O_3 and Ga_2O_3 and an array of C-70 single crystal nanowires have been synthesized by sol–gel chemistry in a porous alumina template.

A simple way of manufacturing nanomaterials using porous alumina is by using electrodeposition. P. Chennapragada [25] synthesized palladium nanoparticles in commercial porous alumina templates using said method. Pores within these nanoporous membranes act as templates for the synthesis of nanostructures of the desired material. T. Gao et al. [27] fabricated large-scale copper nanowires by potentiostatic electrochemical deposition (ECD) of copper sulfate solution within the nanochannels of porous anodic alumina templates. They emphasize on the importance of applied potentials during the process. Lower potentials were necessary to prepare single crystal copper nanowires and to avoid formation of copper oxides in the pores. J. Oh et al. [33] electrodeposited Cu_2O nanowires using their own manufactured alumina templates. Their objective was to use them for solar cells and sensor applications but failed to meet high aspect ratios and compactness.

Y.C. Sui et al. [7] successfully synthesized carbon nanotubes in porous alumina templates anodized in sulfuric and/or oxalic acid solution. Following their experimental procedure, the anodic films were cleaned in boiling water carefully after anodization. Pairs of alumina templates with or without boiling in water where used. Carbon nanofibers and nanotubes where then synthesized by acetylene pyrolysis at 650 and 550ºC. According to the researchers, for templates anodized in oxalic acid followed by boiling in distilled water, thermal decomposition of acetylene at 650ºC in the pores resulted in the formation of carbon nanofibers. For templates anodized in sulfuric acid, only carbon nanotubes were formed, even if boiling in water was adopted to process it.

Z.L. Xio et al. [12] report what they claim to be a convenient and inexpensive way to produce a high yield of both alumina nanotubes and nanowires by etching commercial porous alumina membranes in an aqueous sodium hydroxide (NaOH) solution at room temperature. They studied

13

the effects of etching time and solution concentration and characterized the alumina nanotubes/nanowires using a scanning electron microscope (SEM). While testing with NaOH concentrations of 0.1-1.2M, they found that the dissolving process slows down with decreasing NaOH concentration. The researchers also point out a problem with using this method: The similarity of the observed alumina nanotubes/nanowires with the nanowires grown in the pores by electrodeposition calls for special care in characterizing the nanowires with scanning electron microscopy.

Shingubara [11] addresses urgent existing problems in the field of fabricating nanomaterials using porous alumina templates: the pitch of a highly ordered nanohole array formed by self-organization is still limited; a method to control nanohole diameters below 5 nm for observing the quantum confinement effect has yet to be devised and; a fabrication procedure for integrating porous alumina nanohole membranes on semiconductor solid substrates, while at the same time maintaining their mechanical stability, has not yet been established.

2.2.4   *Nanoporous Templates*

Nanoporous templates have been developed and fabricated using track etching technology on polymer films or polymer layers deposited on varied substrates like wafer, glass or metal. These templates are useful for the synthesis of metallic or polymeric nano-objects and are therefore used for the growth within their pores of arrays of controlled nanowires. [24]

M. Toimil et al. [17] achieved electrochemical deposition of copper nanowires in etched ion tracked membranes using a simple salt electrolyte. Polycarbonate discs were irradiated with highly charged gold and lead ions. These ions created cylindrical damage zones that were later etched away to create cylindrical pores. Typical electrochemical deposition was performed to

deposit the copper in these pores and create nanowires. The wires had diameters between 60 and 500 nm and aspect ratios of up to 500. The author states that this method opens up the possibility of comparing the influence of poly- and single-crystallinity on transport processes in nanowires, for example the flow of electric current and propagation of sound waves.

The same author continued experimenting different parameters using this type of template. Further studies showed the importance the conditions during the electro-deposition. The presence of air bubbles in the pores, overvoltages or bad quality deposition at high currents caused large roughness of the wire surface. Single crystalline wires grown at high temperatures and low voltages possessed homogeneous and smooth surfaces. [19] The team went on to study the electrical properties of the wires, finding that the wire resistance varies between a few hundred ohms and several megaohms, enabling its usage as metallic or semiconducting structural elements for devices on the nanometer scale. [20]

2.2.2   Powder Templates

Córdoba and Odén [3] studied flat glassy carbon and graphite powder as substrates to deposit copper via electroless deposition. The graphite was coated with copper over a range of synthesis conditions, and a dense, homogeneous copper coating was obtained. Copper was only present on the glassy carbon substrate when short deposition times or low pH were used. The authors point out that this was probably due to the fact that none of the pretreatments used resulted in good Sn impregnation of the glassy carbon surface and copper is reduced in the solution instead of being deposited on the surface.
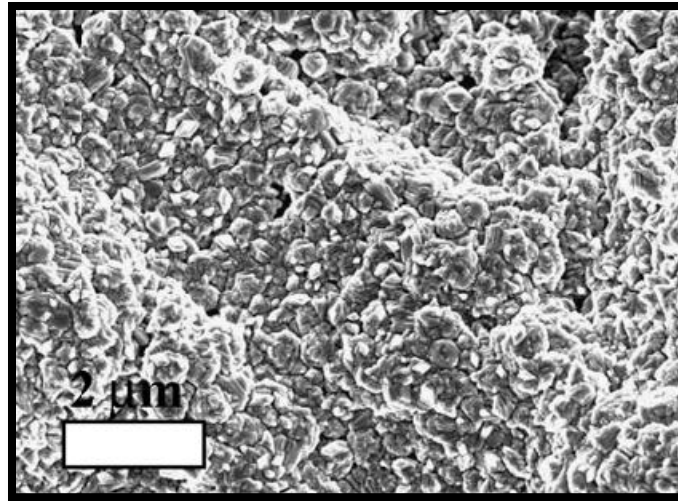
Figure 2.4: Glassy Carbon sample after Cu coating [3]

Whilst studying the importance of nanocoating and nanocomposites, Q. Chen [9] developed a method in which the surface of commercial titania (TiO$_2$) nanopowder was coated with a layer of silica by a two-step process which involved power ultrasound initiated sol gel reaction. In the first step, aminosilane was used to modify the surface of the nanoparticles. Silica nanocoating was initiated and sustained under power ultrasound agitation in a mixture of surface modified particles and epoxysilane. Application of power ultrasound fulfills two functions: it initiates and sustains reactions leading to growth of silica, and helps in keeping the nanoparticles dispersed in solution. As a result, the author says they obtained a homogenous coverage of silica on the nanoparticles' surface, with thickness controllable from one to several nanometers.

S. Shukla et al. [35] used fly ash cenosphere particles and coated them with copper by means of electroless copper deposition. In their experiment, however, they replaced the conventional palladium salt activator with AgNO$_3$ to reduce the cost of the process.

2.2.3   Nanofiber Templates

Nanofibers themselves have been used to fabricate nanowires of different materials. Tao et al. [2] prepared polyamide 6 (PA6) nanofibers by means of electrospinning. Electroless deposition was then used to deposit copper on the surface of the fibers. Using scanning electron microscopy revealed the uniform coating of the PA6 nanofibers with thin films of Cu. Surface resistance of the coated nanofibers was also measured to be 24.41 ohm/sq.
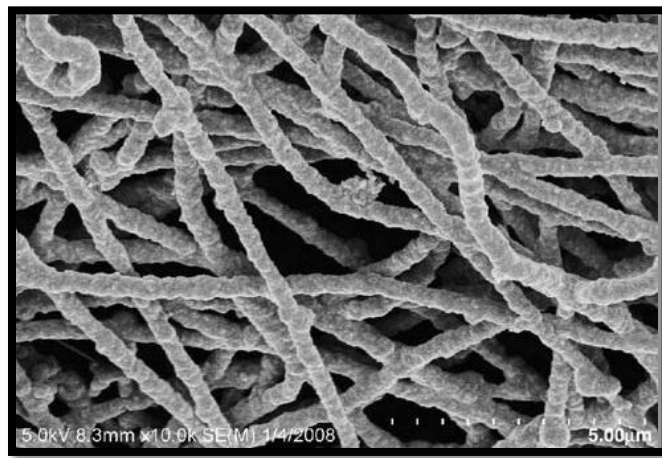
Figure 2.5: Electrospun PA6 fibers after Cu electroless deposition [2]

Córdoba and Odén [3] used carbon nanofibers with two different microstructures, herringbone and platelet, and used electroless copper deposition to deposit copper on the surface of the fibers. Their study shows the importance of the pretreatment of the fibers, since the surface condition of the substrate affects all subsequent steps. Their conclusions state that the best coatings were obtained for a pretreatment in boiling acetone and $H_2SO_4/K_2Cr_2O_7$ of the fibers with herringbone structure, and using a coating bath with pH 12 at room temperature.

H. Xing et al. [5] achieved multifunctionality of carbon nanomaterials using electroless deposition of nickel. Synthesis of magnetic Ni coatings on individual carbon nanofibers and

nanotubes was realized through solution penetration and ion diffusion. Their results indicate a significant improvement of the fibers' electrical conductivity and a magnetic response which can be tuned within large ranges in terms of saturation magnetic field. After being re-suspended in liquids, the magnetized nanotubes and nanofibers can be aligned with small external magnetic fields. The authors point out that these hybrid carbon nanostructured materials have broad applications in reinforced nanocomposites, EMI shielding materials, fuel cell electrodes, catalysts, supercapacitors and bio/chemical sensors.

An Bargang et al. [26] demonstrated that nickel could be deposited on the surface of carbon nanotubes without pre-sensitization by Sn^{2+} and Pd^{2+}. They attribute this to the high concentration of nanotubes suspended in their bath that formed a continuous net between the cathode and the anode.

K. Valenzuela et al. [14] used electroless copper deposition to produce copper nanowires by metallizing microtubules. These nanowires would be used for applications such as electrical nano-interconnects. Since microtubules are poorly conductive their use as interconnects necessitates metallization. They report that control of the pH levels was critical at the moment of ensuring proper metallization and to avoid destroying the template. They concluded that their approach enabled the use of microtubules as templates for manufacturing copper nanowires with 15 nm diameters.

Ugur et al. [13] produced carbon nanofibers with Platinum and Palladium nanoparticles from a Polyacrylonitrile solution by electrospinning and subsequent pyrolysis in a tube furnace with controlled atmosphere. Nanometer size zero-valent Pt and Pd atoms were precipitated selectively

on nanofibers from a PdCl$_2$ and H$_2$PtCl$_6$ solution in the presence of hydrazine by using electroless plating techniques at ambient conditions.

Researchers like A. Buldum et al. [37] have used nanofibers as templates by coating them with metallic materials using plasma enhanced physical vapor deposition. In the end, they eliminate the nanofibers to create nanotubes of the selected metal.

J. Lim et al. [36] used PAM, PEO and PAN electrospun nanofibers as confining geometries for fabricating silica assemblies. By dispersing silica particles in the polymer solutions, the particles assembled spontaneously into a pearl-necklace structure.

2.3   Nanomaterials as Lead-free Technology

Already nanomaterials are being studied as potential lead-free solder candidates. H. Jinag et al. [28] state they synthesized tin/silver alloy nanoparticles with various sizes by the chemical reduction method for lead-free solder applications. Their thermal properties were studied by differential scanning calorimetry. Both the particle size dependent melting temperature and latent heat of fusion have been observed. The melting point can be achieved as low as 194°C when the diameter of the nanoparticles is around 10 nm. The 64 nm (average diameter) SnAg alloy nanoparticle pastes showed good wetting properties on the cleaned copper foil surface and the intermetallic compounds formed.

S. Joo and D.F. Baldwin [18] studied how silver nanoparticles could be used as interconnect material in electronic packaging. The silver nanoparticles are around 8nm in diameter and are sintered at a temperature of 230°C for an hour with rapid cooling to form a material nearly indistinguishable from bulk silver. The resistivity of the silver nanoparticles was identified to be

about 6 μΩ cm, comparable to bulk silver's resistivity of 1.6 μΩ cm. Adhesion test results indicated that the processed silver nanoparticles had excellent adhesion with polyimide, liquid crystal polymer (LCP), and copper. The authors conclude that these results confirm that the silver nanoparticles show reasonable performance as microelectronics packaging interconnect materials. In addition, improvement and control of the adhesion strength of NPS to packaging materials would be a key factor for improving the reliability of the rapid package prototyping technology.

Alloys themselves are being taken to nanoscale. L.Y. Hsiao et al. [32] synthesized lead-free solders with SAC nanoparticles by the chemical reduction method. TEM images revealed that the sizes of the isolated and polycrystalline particles are about 5 and 40 nm, respectively. The melting point of the SAC nanopowders was reduced to 215°C. The nanopowders derived from the chemical reduction method could be employed as solder materials for the subsequent reflow process along with the wettability test.

K. M. Kumar et al. [30] reinforced SAC solders with single walled carbon nanotubes, nano-nickel and nano-Mo by using a powder metallurgy method. When compared to the SAC solder without any reinforcement, the composite solders exhibit enhanced hardness, enhanced yield strength and enhanced ultimate tensile strength. However, the elongation to failure of the composite specimens considerably decreased. The increase in the strength of the nanocomposite solder specimens can be attributed to the critical reduction in the grain size. The enhanced mechanical properties also can be attributed to the effective load-transfer between the solder matrix and the nanotubes.

S.M.L. Nai et al. [31] had similar results when reinforcing SAC solder with multiwalled carbon nanotubes. Mechanical characterization results revealed that the presence of increasing weight percentage of CNTs in solder matrix led to overall improvement in microhardness, 0.2% YS and UTS. However, ductility of the composite solders was found to slightly decrease.

2.4 Application of Literature Review

From this review, an approach is taken in which electroless copper deposition will be used as the preferred method of coating polymer nanofibers to produce copper nanoparticles due to the procedures ability to deposit metal on the non-conductive surface of a polymer nanofiber. These nanoparticles will be tested to see if they can be used as a feasible nano-solder substitute for lead based solders.

CHAPTER 3: METHODOLOGY

Polyacrylonytrile nanofibers were coated with copper by electroless deposition. Each step of the process was carefully monitored to ensure proper and efficient samples of nano-sized copper were being manufactured. Once prepared, they were tested for melting point and mechanical properties in order to determine their potential as lead-free solder.

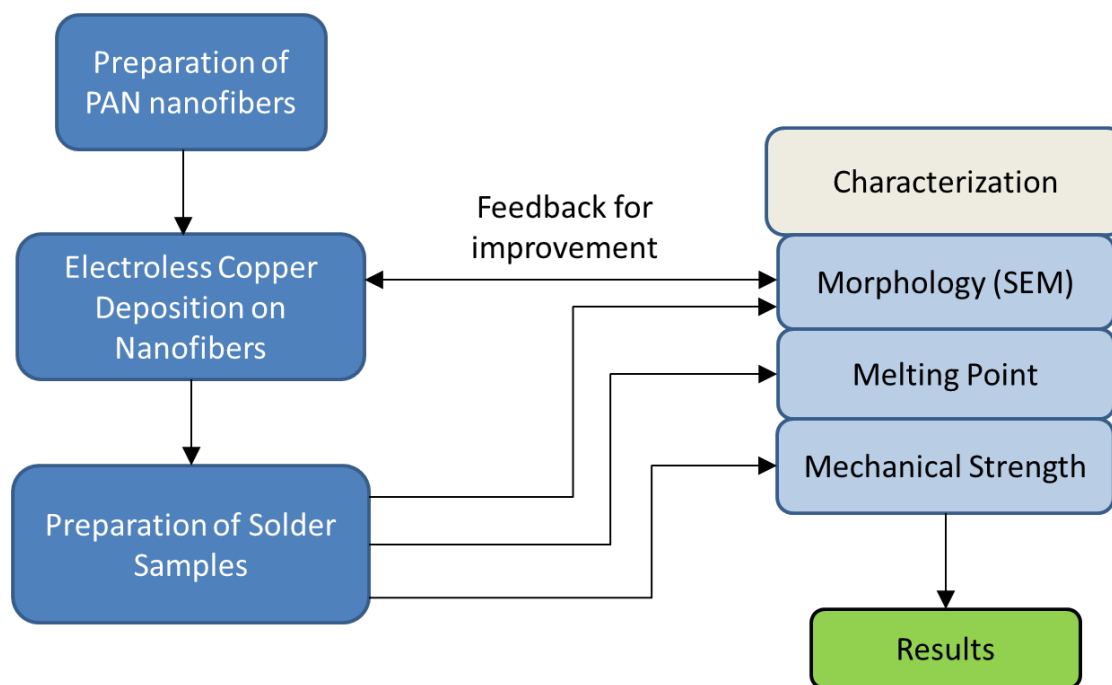**Figure 3.1: Experimental Procedure for Preparation and Characterization of Lead-free nano-solder.**

The figure above summarizes the methodology for this research. First the nanofibers are prepared for the electroless plating. The plating process is repeated, studied and tested until a functional, standard procedure is achieved. Melting point is measured to prepare specimens for further mechanical testing.

3.1 Preparation of Nanofibers

Polyacrylonitrile (PAN) nanofibers were used as the templates on which to deposit copper on. PAN solutions of 10%wt were prepared by simple dissolution of the polymer in dimethylformamide under constant agitation. Electrospinning was then performed to produce the nanofibers from the solution. Figure 3.2 shows a diagram of the electrospinning setup used at the laboratory including the dispersing syringe, the collector and power source.
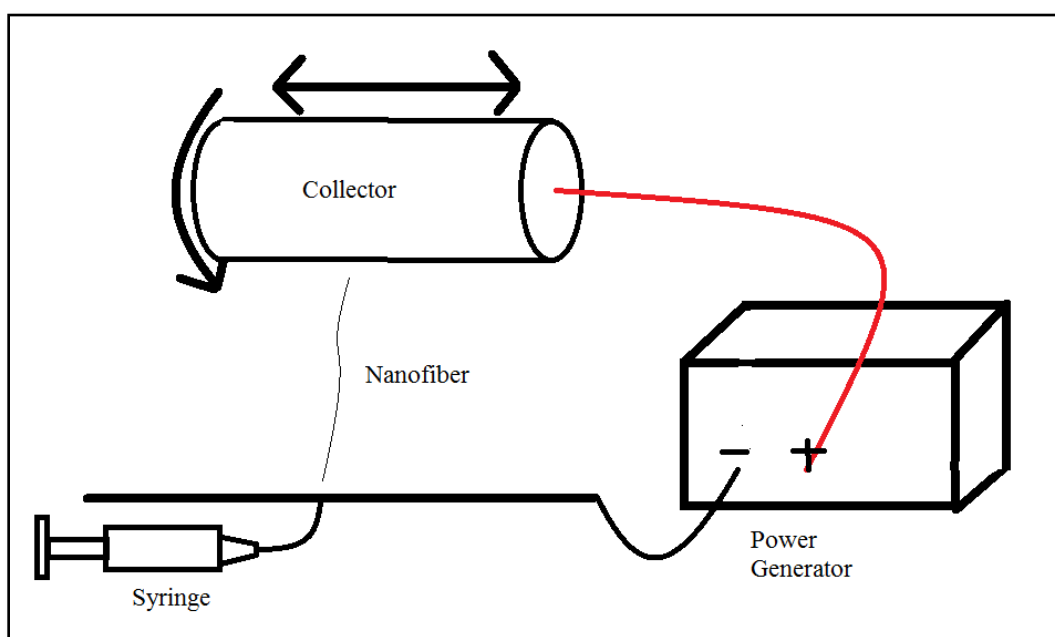
Figure 3.2: Electrospinning setup.

The solutions were dispensed using a 3 ml syringe and a blunt tip needle of gauge 23. The anode of a high voltage power supply was clamped to a syringe needle tip, and the cathode was connected to a rotating central collector. When the power supply was turned on and the syringe was pumped, fibers were collected on the collector. Microscopy was used to determine the initial nanofiber diameter before plating the samples.

3.2 Electroless Copper Plating

The basic problem in attempting to electroplate onto plastics templates is that they are electrically non-conductive and cannot be immersed in a plating solution and coated the same way metal objects can by electroplating. A method is therefore needed whereby a conductive film can be deposited onto the plastic's surface to provide the basis for subsequent electrodeposition. This surface layer, in addition to being electrically conductive, should adhere well to the substrate if the final coating system was to show good adhesion. [8] To coat the nanofibers with copper to obtain the potential nano-solder, the electroless deposition technique was used.

The electroless copper deposition process consists of various steps, each having its own solution. These are: pre-treatment, sensitization, activation and coating. A design of experiment was performed in order to optimize the electroless plating process. The variables changed were temperature, time and pH level as shown in Table 3.1.

Table 3.1: Design of Experiment Variables for Electroless Copper Plating

Plating Step	Time	Temperature	pH level
Pre-treatment	5,10 minutes	Ambient, 60°C	N/A
Sensitization	5,10 minutes	N/A	N/A
Activation	5,10 minutes	N/A	N/A
Coating	15, 30 minutes	Ambient, 60°C	7,10,12

Figure 3.3 illustrates the experimental setup used for the electroless plating process. Each sample of nanofibers was submerged in each solution for a determined amount of time and

rinsed afterwards. Solutions are in constant stirring when a sample is submerged by using a magnetic stirrer. The heater included in the equipment is used when temperatures are needed to be raised accordingly.
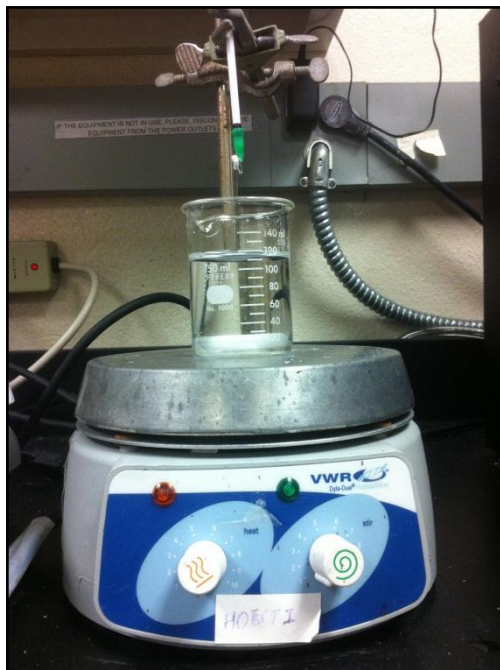

Figure 3.3: Experimental Setup for Electroless Copper Plating

The following sections will describe each of the steps in detail as how they were performed. All chemical solutions are designed after the solutions studied in the literature review.

3.2.1   Pre-treatment

The pre-treatment starts with cleaning the fibers. This ensures that the surface of the fibers is free from any contaminants that may hinder any proper adhesion in the remaining steps. Cleaning of the nanofibers is done by dipping in acetone for 5 minutes and rinsing with distilled water.

Pre-treatment includes etching of the surface. Etchants are usually strong oxidizing solutions that eat away the surface to varying degrees, accomplishing two purposes. First, the surface area

is greatly increased, making the part turn from a hydrophobic (water-hating) to a hydrophilic (water-loving) material. Second, the holes left on the surface of the fibers by the etchant provide the bonding sites for the deposited metal. These sites are needed for adhesion between the fiber and the metal. [10] The figure below shows a visual representation of the effects of cleaning and etching.
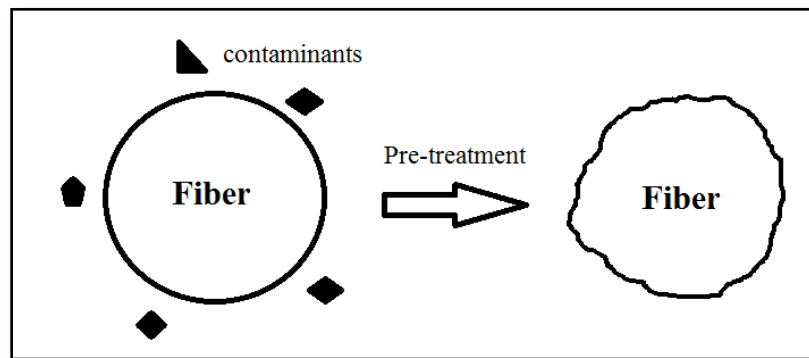

Figure 3.4: Pre-treatment -- Cleaning and Etching.

The etchant solution consists of 15 g/l $KMnO_4$ and 40 ml/l H_2SO_4 and the bath takes around 3 to 5 minutes to successfully etch the surface, meaning the surface has been properly roughened and anchor sites have been made for subsequent palladium placement.

3.2.2   Sensitization and Activation

Proper activation is perhaps the key step in the electroless copper process, other than the electroless deposition itself. Activating solutions (or catalysts) typically contain palladium held in a reduced state by stannous ions. These solutions are typically high in chloride ion and possess some degree of acidity. The figure below illustrates the effects of sensitization and activation:
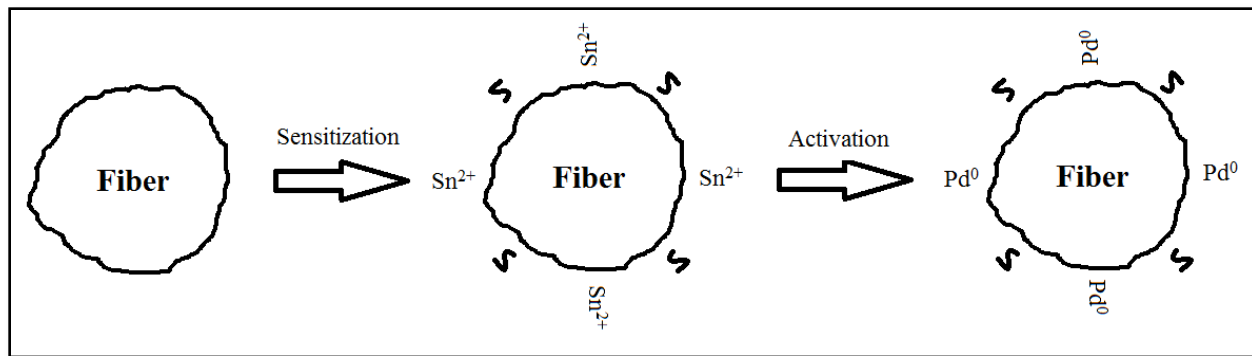
26

Figure 3.5: Sensitization and Activation.

Activation is a two-step procedure. Step 1 is a stannous chloride/hydrochloric acid solution (0.5M hydrochloric acid with 0.034M $SnCl_2$ $2H_2O$ for 2-5 mins.) in which the stannous ion (Sn^{+2}) is adsorbed onto the surface. This is sometimes better known as the sensitization solution. The fibers are then rinsed well with distilled water. Step 2 is a palladium chloride/hydrochloric acid solution (2.5ml/l hydrochloric acid containing $5x10^{-4}$ m $PdCl_2$ for 5 mins.) which causes the Pd^{+2} ions to be reduced to Pd^0 according to the following reaction [10]:

$$Sn^{+2} + Pd^{+2} \rightarrow Sn^{+4} + Pd^0$$
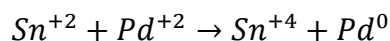
The Pd sites form the catalytic surface needed to deposit the copper. The palladium activation solution is the most expensive solution because of the palladium used; however, only one solution was needed to produce the dozens of samples prepared during the investigation.

3.2.3 Coating (Electroless Deposition)

After rinsing, the fibers are put into the electroless bath, which deposits a thin, adherent metallic copper film on the plastic surface by chemical reduction. This is accomplished by using a semi-stable solution containing a metal salt, a reducer, and a complexor for the metal. When idle, the

27

bath is stable, but when the palladium-bearing surface is introduced into the solution, a chemical

reduction of metal occurs on the palladium sites. The basic reaction for the copper is [10]:

$$Cu^{+2} + 2HCOH + 4OH^- \xrightarrow{Pd} 2HCOO^- + 2H_2O + Cu^0 + H_2$$
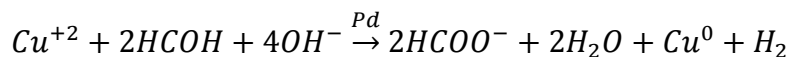
The coating solution will consist of 0.1M $CuSO_4$ $5H_2O$ (metal source), 0.2M $KNaC_4H_4O_6$ (complexing agent) and 5ml/l HCHO (reducing agent) (Figure 3.6).
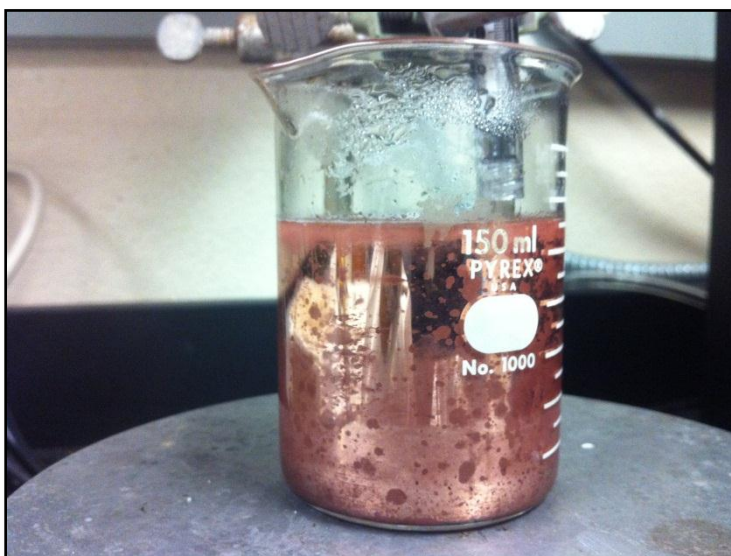

Figure 3.6: Successful Reduction of Copper in Coating Solution.

Temperature is raised to 60°C and pH is controlled by adding NaOH pellets. Various

experiments revealed that both temperature and pH parameterization determine if there is

constant and efficient reduction of the copper.

The visual representation of the coating step can be seen in the figure below:
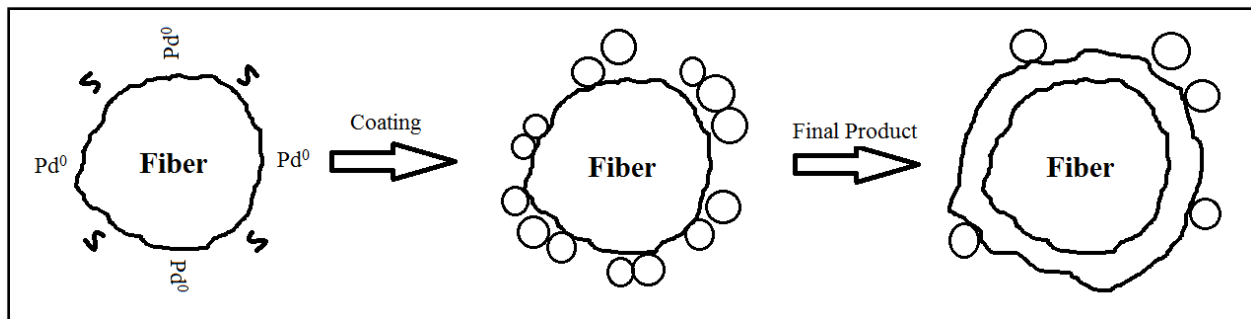
Figure 3.7: Coating Step and Final Product

The table below summarizes the steps of the electroless copper plating procedure performed for this research:

Table 3.2: Electroless Copper Plating Steps and Solutions

Steps	Description	Solution
Pre-Treatment	Removes any contaminants. Etching for better anchoring sites for the activator.	Acetone for 5 mins. For etching: 15 g/l $KMnO_4$ and 0.75 M H_2SO_4 for 3 mins.
Sensitization	Gives better adherence.	0.5M HCl with 0.034M $SnCl_2$ $2H_2O$ for 2-5 mins.
Activation	Activation of the surface	0.08M HCl containing $5x10^{-4}$ M $PdCl_2$ for 5 mins.
Coating	Coating of Cu with the electroless plating bath	0.1M SO_4Cu $5H_2O$ (metal source), 0.2M $KNaC_4H_4O_6$ (complexing agent) and 0.18M HCHO (reducing agent)

3.3   Characterization

Several methods were used to characterize each sample with the purpose to optimize the production and ensure that they meet the requirements a lead-free solder should have when replacing the current lead based solders. Each method is described in the subsequent sections.

3.3.1   Scanning Electron Microscopy

A scanning electron microscope was used to obtain images of the nanofibers before and after coating. This allows monitoring of the electroless plating process and whether it is properly coating the fibers with copper. Initial and final dimensions can also be obtained to determine the particle size of the copper. Morphology was also observed and studied. Energy dispersive spectroscopy (EDS) was used to confirm the presence of copper on the fibers.

Figure 3.8: Scanning Electron Microscope (SEM), University of Puerto Rico at Cayey

3.3.2 Melting Point

First, a control sample is heated to the bulk copper melting point temperature using the equipment shown in Figure 3.9. This will ensure that the sample has completely melted. The sample is later observed on the SEM and the image used as a reference to compare with later samples in order to determine whether said future samples have reached the nanomaterials melting point.

Figure 3.9: High temperature oven used in experimentation.

To determine the melting point of the copper after the electroless plating, several samples were heated in an oven at various temperatures ranging from 200 to 1000°C. Each sample was then observed at the SEM to determine a range of temperature in which the copper melts by observing the morphology and comparing it with the control sample. This melting temperature range was to be later used to prepare samples for mechanical testing.

3.3.3 Mechanical Strength

The lap-shear technique is widely used to evaluate the shear, creep, and thermal fatigue behavior of tin–lead and Sn-rich solder joints. The general deformation mode mimics many real-life loading configurations of solder joints. The solder is placed between two metallic substrate blocks, which are pulled in opposing directions to provide shear loading. [44] A similar test is performed to test how much stress the solder manufactured in the laboratory can withstand before failure. Figure 3.10 shows the tensile strength tester used in the laboratory; a Mark-10 tensile tester including an ESM stand with force gauge.

Figure 3.10: Tensile Strength Tester

Once the temperature range at which the copper samples melt is determined, two copper strips are soldered together using the potential nano-solder as seen in Figure 3.11. In order to achieve adherence, flux was applied. Without flux, the nano-copper would just melt between the copper strips without joining them.

Figure 3.11: Copper Strips joined together by nano-copper solder.

A design of experiment was implemented to test different specimens heated at different temperatures for different times. The table below summarizes the variables and their values.

Table 3.3: Design of experiment variables for mechanical testing

	Temperature	Time
Value 0	600°C	5 seconds
Value 1	700°C	10 seconds
Value 2	800°C	20 seconds

Literature review suggests that at these temperatures the PAN nanofibers are calcinated, leaving behind copper nanotubes with no fibers inside. The structure left however can be beneficial in improving the mechanical strength of the solder, simulating reinforcement of nanofibers added to SAC solders.

CHAPTER 4: EXPERIMENTAL RESULTS

The following chapter will summarize all the results obtained during the research. Results focused on determining the copper particle size, the melting point of the copper particles and the mechanical strength of the product used as a solder.

4.1 Pre-process Nanofibers

The Polyacrylonitrile (PAN) fibers were observed at a SEM microscope to determine their initial size before the electroless plating process.
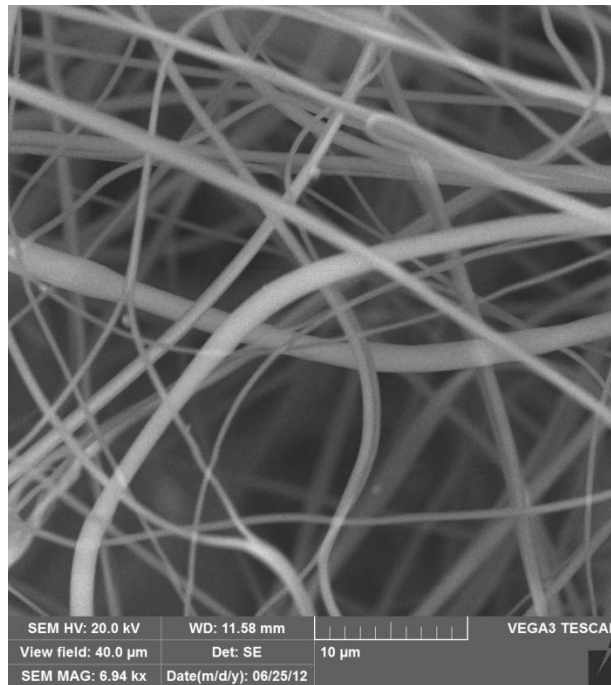

Figure 4.1: SEM image of PAN nanofibers.

Fibers had an average diameter of 500 nm and 1000 nm. Using these values it is possible to later determine the thickness of the copper layer that would deposit over the fibers.

4.2 Electroless Copper Deposition

Following the design of experiment described in the previous chapter, several observations are performed to optimize the electroless copper plating of the nanofibers.

Cleaning of the fibers demonstrated to be essential, as adherence of the copper depends on whether the surface of the fibers was clear of any obstruction. Skipping this step would mean failure even when performing subsequent steps perfectly. For etching, neither time nor temperature presented difference in results. Previous works like the ones mentioned in Chapter 2 done by Córdoba suggest that etching time be less than 5 minutes to avoid damaging the fibers in excess.

Experiments for sensitization and activation steps showed that 10 minutes was optimum to ensure proper activation. Experimentation also showed the importance of these two baths. Figure 4.2 shows two membranes, both which were inserted in the plating bath, but the membrane without proper activation, thus no palladium, had no plating of copper at all.
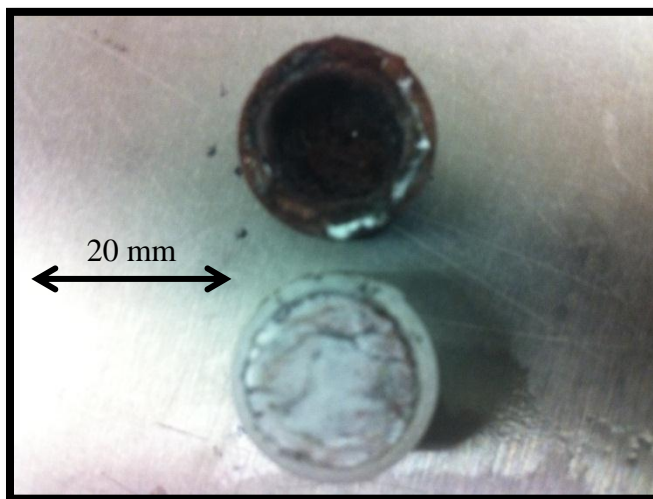

Figure 4.2: Membranes inserted into plating bath with activation (above) and without activation (below).

The coating bath had more factors to be considered. Bath time was dependent of the time it took the solution to reduce the copper, so other factors like temperature and concentrations were studied to see what affected said reduction. Elevated temperatures (in this case 60°C) helped accelerate the reaction and promote successful results.

The pH level was the dominating factor in determining whether a solution would provide good results. Different pH caused different effects as evidenced by the different colors (blue, light blue, green) the solution would take at different pH values as seen in Figure 4.3. Clear and effective reduction of copper was found to be achieved when the pH was kept in a range of 11-12.

Figure 4.3: Coating solutions at different pH levels.

Not having the solutions at a basic pH would cause the solution to either produce copper oxide instead of metallic copper, resulting in a green solution, or not deposit copper at all, causing the solution to become light blue.

The table below summarizes the results obtained after experimenting determining the best values the variables of the design of experiment should have for proper copper plating.

Table 4.1: Results for Copper Plating Variables

Plating Step	Time	Temperature	pH level
Pre-treatment	5 minutes	Ambient	N/A
Sensitization	10 minutes	N/A	N/A
Activation	10 minutes	N/A	N/A
Coating	15 minutes	60°C	11-12

After taking the fibers through the electroless copper plating process, the samples were dried and images were taken to make measurements. The first observations were, of course, the macroscopic views of the fibers.

Figure 4.4: Nanofibers before (left) and after (right) the electroless copper plating.

Figure 4.4 shows two membranes showing the effects of the electroless copper plating. The nanofiber membranes acquire a brown color caused by the adhered copper. Membranes will start turning green as the copper oxidizes.

4.3 Microscopy Characterization

First observations of the coated fibers were made using an optical microscope. With the images obtained, it was possible to determine the effective final diameters of the fibers.
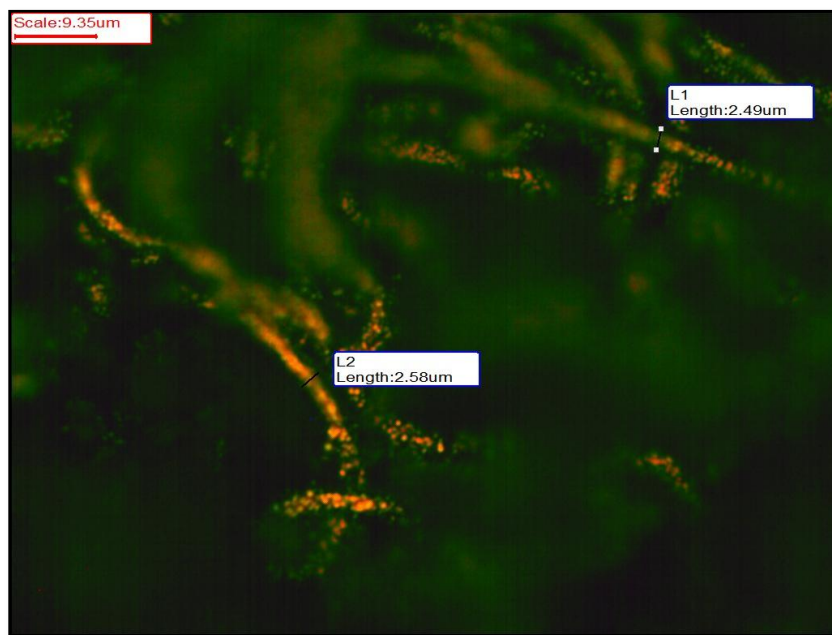

Figure 4.5: Optical Microscope image of coated fibers.

Results show that fibers which had average initial diameters of 500 nm had final diameters of 1000 nm whilst fibers with initial diameters of 1000 nm had final diameters of 2500 nm. Simple calculations therefore show that the effective thickness of the deposited copper layer ranged from 250 nm to 750 nm.

Further morphology study was needed to determine the nature of the copper being deposited on the fibers. SEM microscopy was then employed to have additional understanding of how the copper was being deposited.
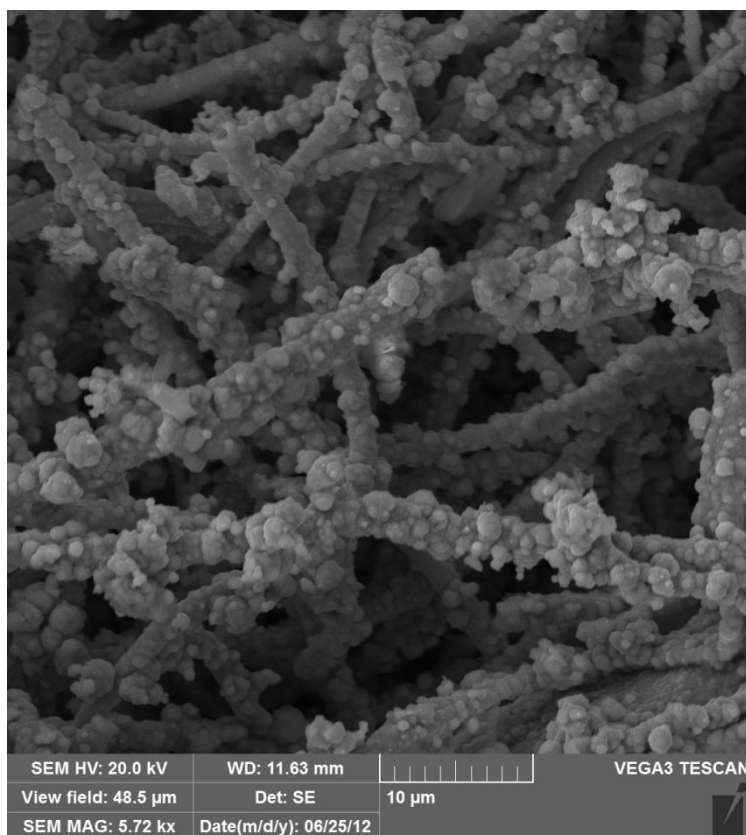
Figure 4.6: SEM image of copper coated fibers (I)

The figure above shows a SEM image of the Cu coated fibers. Coating of the fiber was obtained with additional agglomerates being formed on the surface of the copper layers. These agglomerates averaged at sizes of 500nm-1µm

As can be seen from Figures 7-8, the copper also deposited in the form of agglomerate spheres between the fibers. This may be caused by palladium ions being present between these spaces when the fibers are transferred to the coating solution. Once the palladium activates and starts the reaction, copper starts to nucleate in these spaces. Each sphere is made of smaller individual particles of copper. Spherical growth of copper around the fibers was observed to happen more often than uniform coating as in Figure 4.7. Copper agglomerates that deposited within the membrane but not on the fibers had the largest sizes; ranging from 1-2µm.
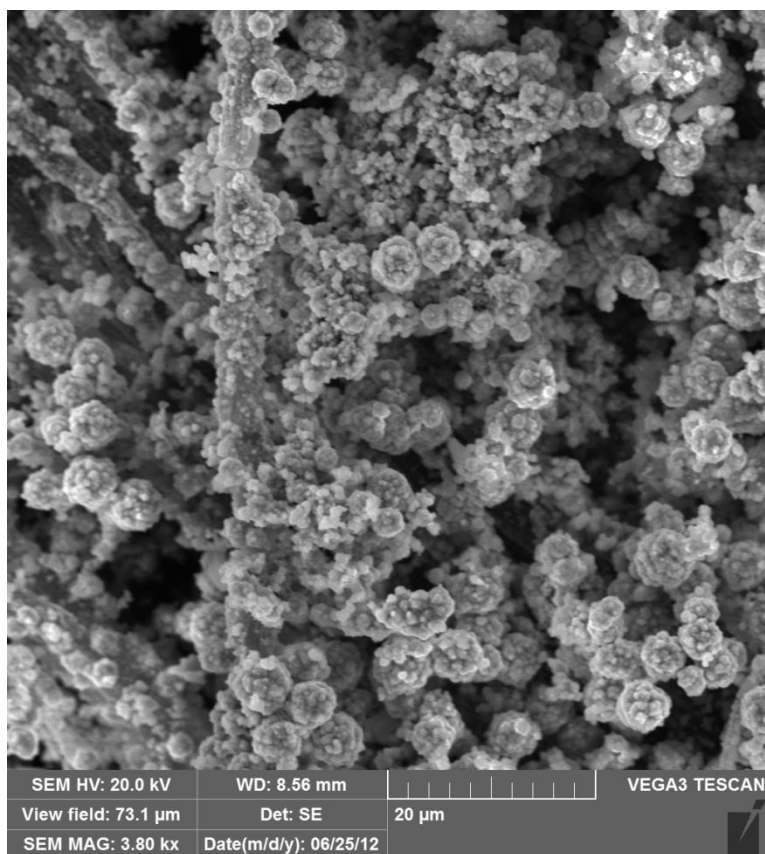
Figure 4.7: SEM image of copper coated fibers (II)

The formation of metal atoms after mixing two solutions under stirring is caused by the transfer of electrons from the reducing agent to the metallic ions. As the nuclei generate in the solution, they undergo rapid diffusional growth at the expense of the remaining atoms in solution and form nanosized primary particles. As more metal atoms are generated in the system, the primary particles may aggregate to form polycrystalline particles with larger sizes. [32]
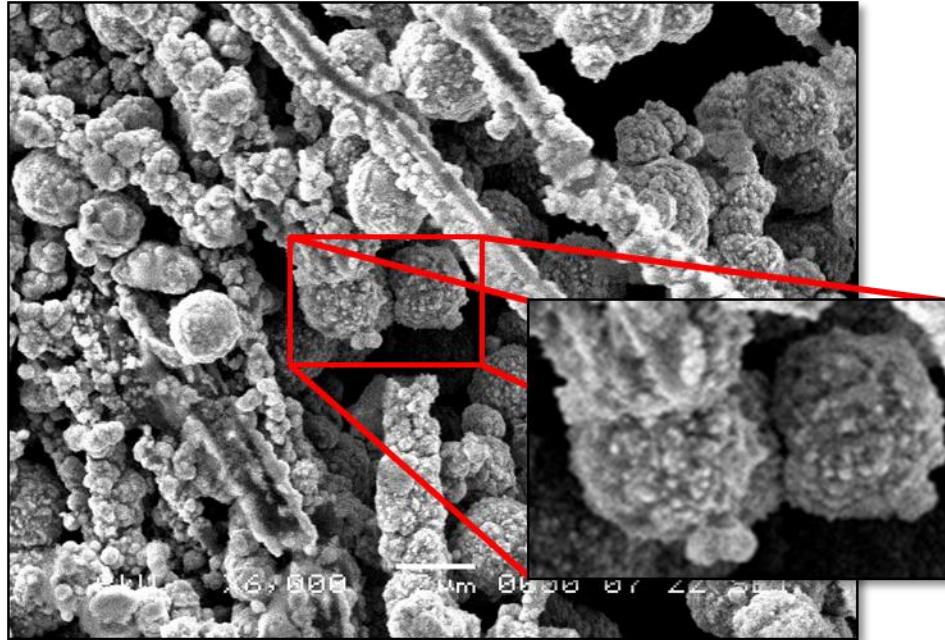
Figure 4.8: Zoomed image of copper agglomerates showing smaller particles around nucleation.

When studying the agglomerates closely, it is possible to measure the copper particles with dimensions of 50-100nm. Although this size range might not provide optimum melting point depression for soldering purposes, it is enough to test whether melting point depression even occurs.

4.4 Energy Dispersive Spectroscopy (EDS)

Using EDS it was possible to confirm that the material being deposited on the fibers was copper.

First, a spectroscopy was performed on clean PAN fibers before the electroless copper process.
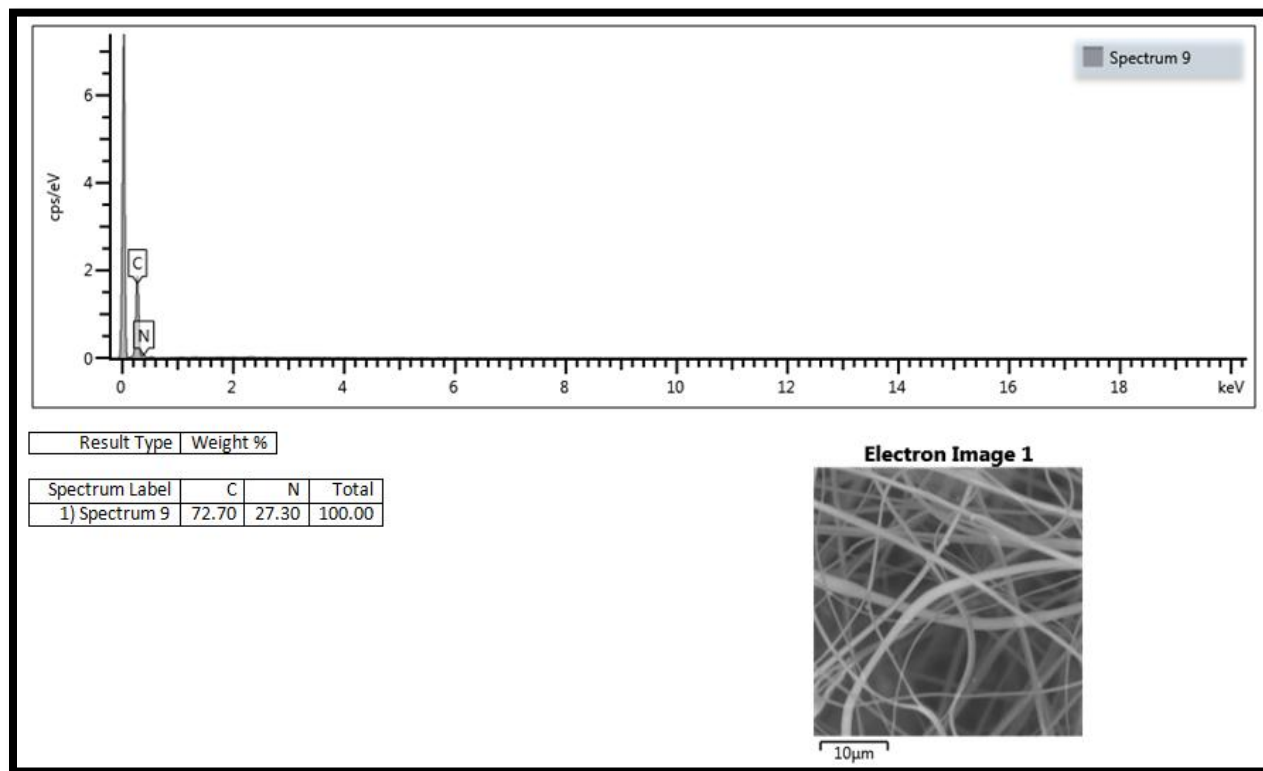

Figure 4.9: EDS of PAN fibers before processing.

Figure 4.9 shows the composition of the PAN fibers, containing 72.70% carbon and 27.30% nitrogen. Following the linear formula of PAN, $(C_3H_3N)_n$ and disregarding the hydrogen weight, mass fractions should be 72% carbon and 28% nitrogen, which corresponds with what the EDS results show.
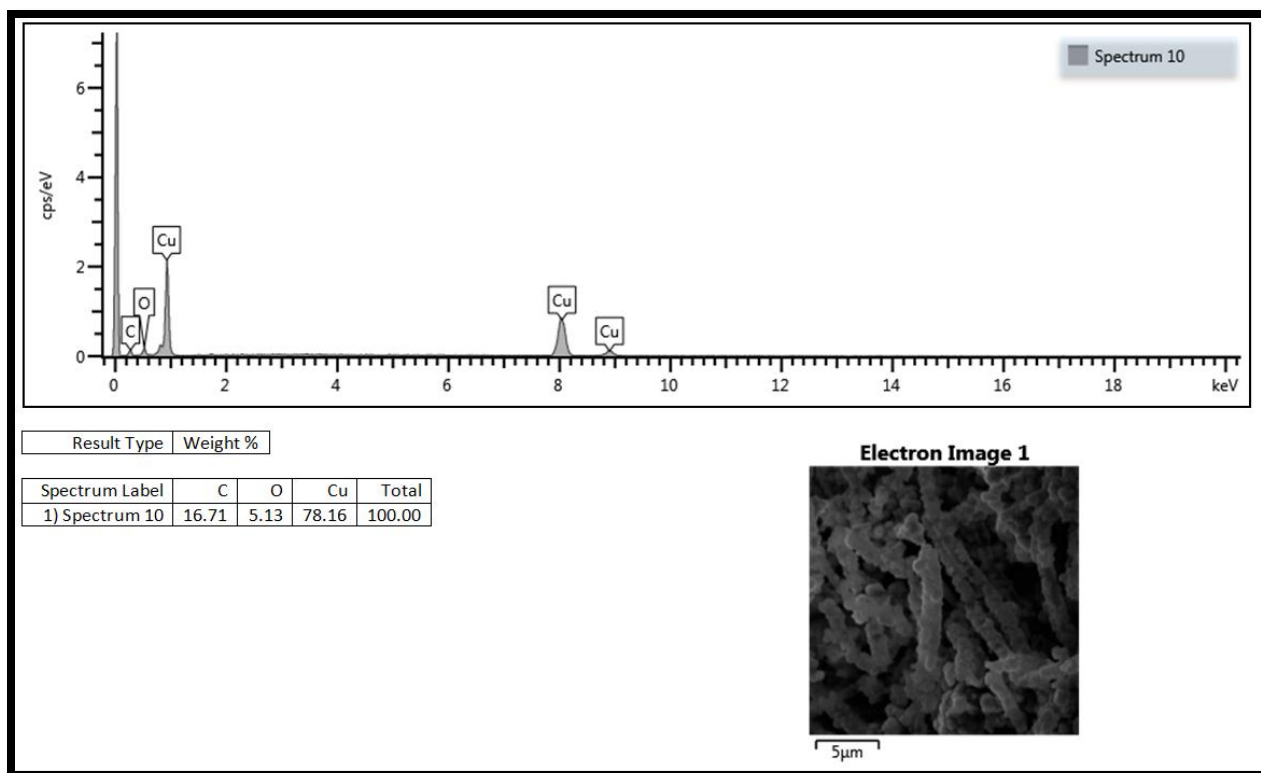
Figure 4.10: EDS of Cu coated fibers.

Figure 4.10 shows the composition of the fibers after the electroless deposition. Presence of copper is evident. Carbon can also be seen present from the fibers. Oxygen presence can be observed due to minor oxidation of the copper due to time.

4.5   Melting Point

The first approach to determine the melting point of the copper coated fibers was to see the effects of heat and temperature on the morphology. Samples were first heated to the melting point temperature of bulk copper (~1084°C) to see their morphology when the copper is melted. Result images of this experiment are below:
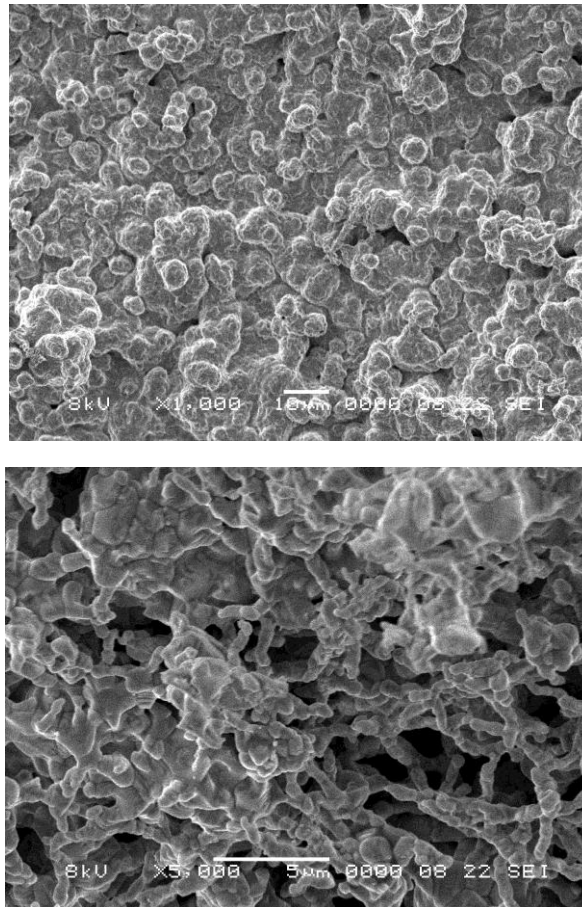

Figure 4.11: Samples heated to bulk copper melting point.

From the images, copper particles which deposited within the membrane melted and became bulk while the copper on the membranes melted along with the fibers, becoming uniform while retaining the fiber's shape.

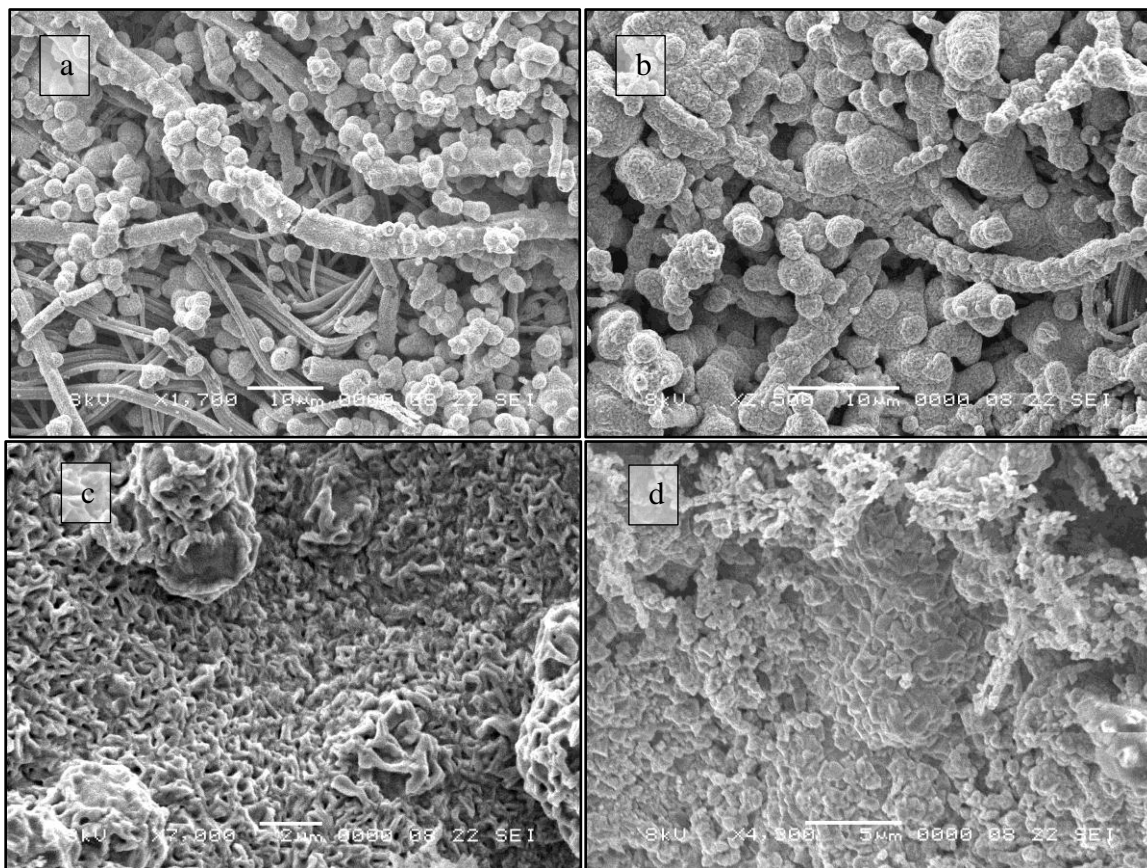From there, samples where heated at different temperatures and their morphologies studied to see any changes.

Figure 4.12: Samples heated at (a) 200°C, (b) 400°C, (c) 600°C, (d) 800°C.

From Figure 4.12, it is possible to see that the melting point of the copper coated fibers is well above 400°C. When the samples are heated at 600°C the copper on the fibers can be seen to take a similar morphology as the fibers heated to the bulk copper melting point. At 800 °C, all copper particles start to form into bulk, suggesting that melting has occurred. These results confirm that melting point depression occurs in the manufactured nano-copper.

As stated in the literature review, previous work has shown that the presence of a template can affect the melting point of a nanomaterial. This could explain why it is possible to see the

45

copper on the fibers start to melt at around 600°C, but complete melting of the copper occurs at 800°C.

As a method of determining the precise moment the samples melt, a thermocouple was placed directly onto the samples while heating them in order to extract a heating curve. Using these curves, it is possible to look for the melting plateau of the material to define its melting point.
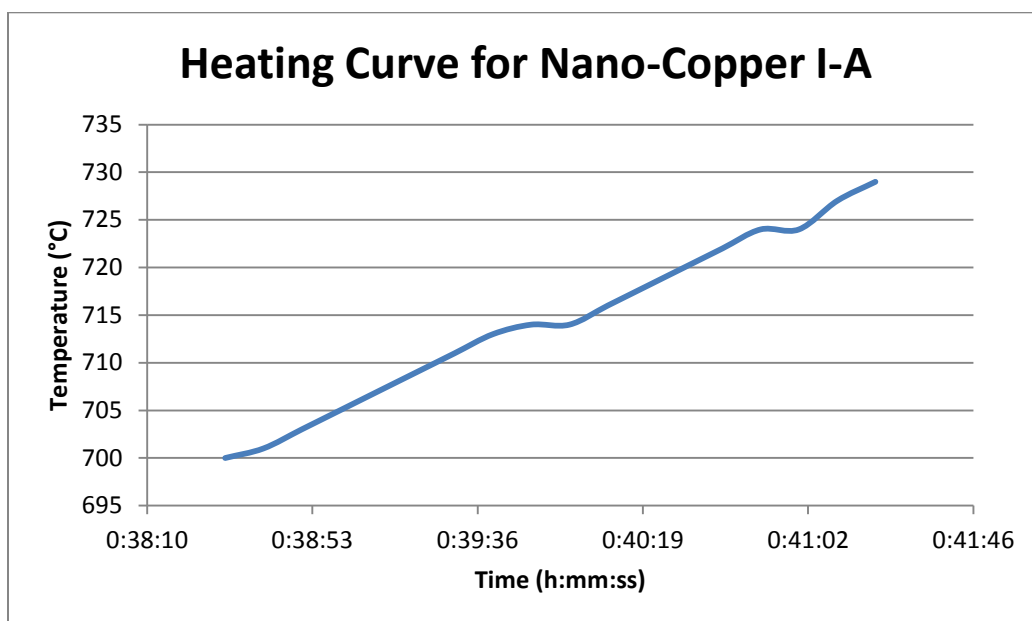

Figure 4.13: Heating curve showing melting points at 714°C and 724°C.

Figure 4.13 shows the heating curve of a sample of the copper coated fibers. As can be observed, two different moments are seen where melting seems to occur in the same sample. This can be attributed to what was observed in the SEM images where different particles at different sizes would melt at different temperatures.

This particular sample had two more plateaus at 838°C and 934°C as seen in Figure 4.14.
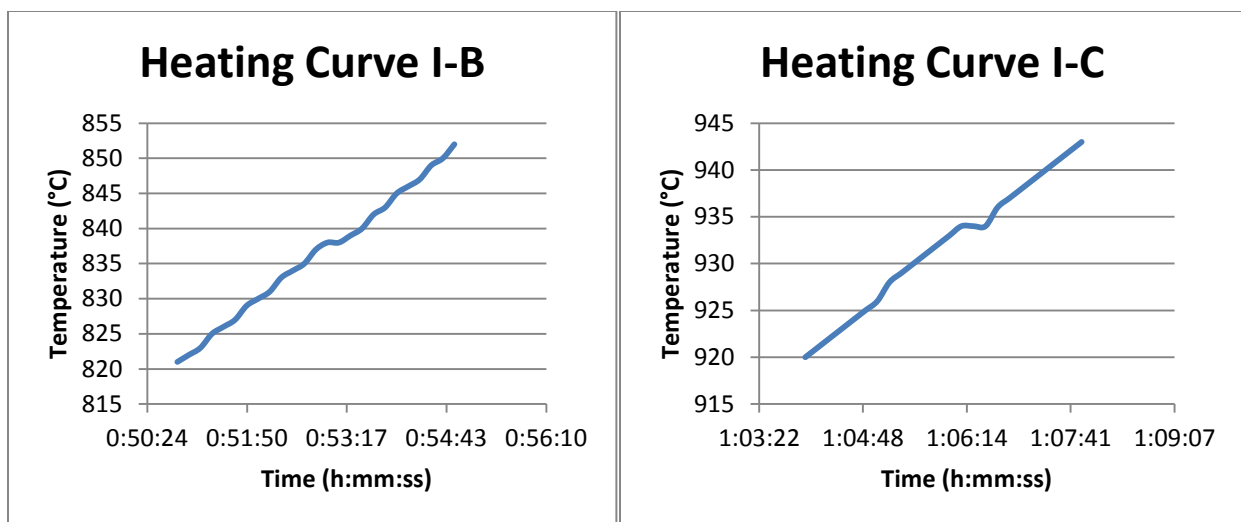
Figure 4.14: Heat curves showing melting plateaus at 838°C and 934°C.

Further testing confirmed the initial melting point range of the material being 600-800°C. The figures below show results for a sample having melting plateaus at 665°C and 813°C.
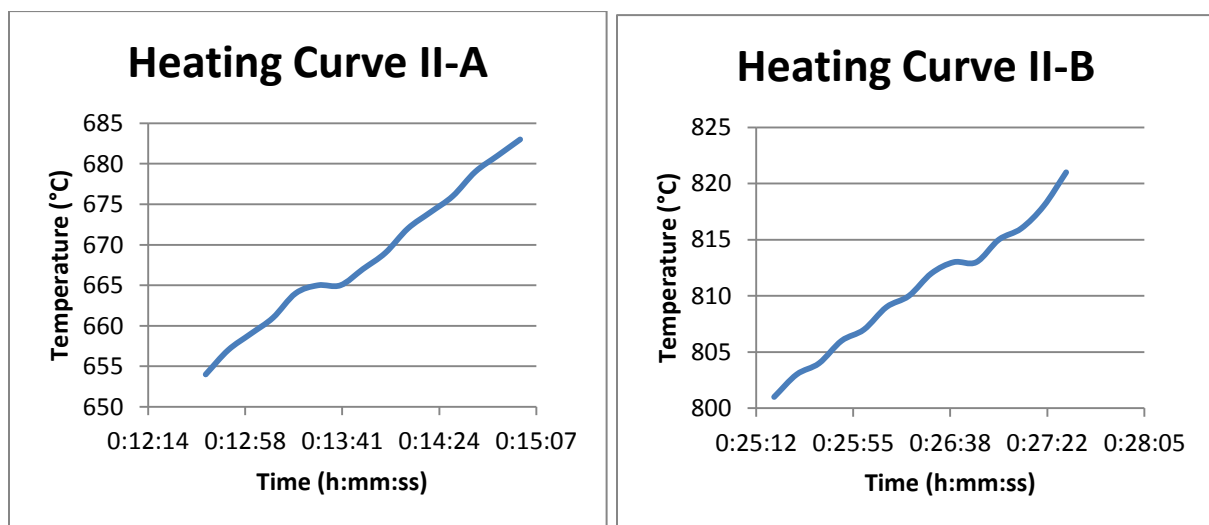

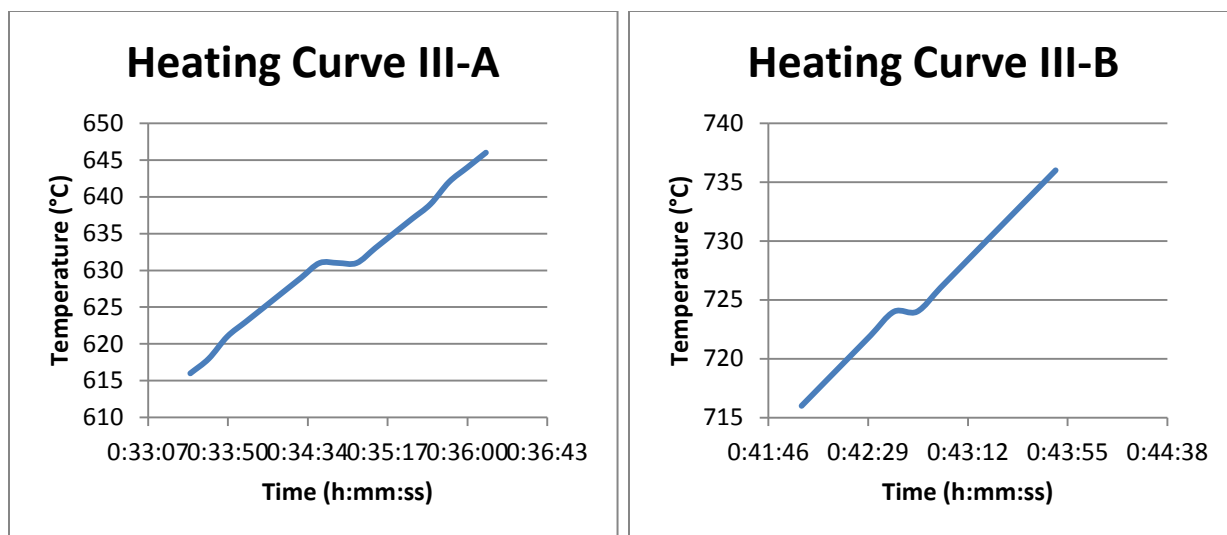**Figure 4.15: Heat curves showing melting plateaus at 665°C and 813°C.**

Figure 4.16: Heat curves showing melting plateaus at 631°C and 724°C.

Two major observations can be made from these results. The first of course is the presence of at least two plateaus in each sample. As explained, this can be attributed to what was observed in the SEM images, which was the presence of smaller particles formed along the fibers and bigger particles formed in-between them.

The second is the variance in melting temperatures between the samples. This is because of the different factors affecting the deposition of copper during their manufacture. The slightest change in temperature or pH levels during the last step in the electroless copper deposition would cause different particle sizes, and therefore, different melting temperatures. However with consistent control of the procedure, the melting temperature of the material could be kept at around 650°C and 724°C.

4.6   Mechanical Strength

Having determined the melting temperature range, samples for mechanical testing could be prepared. Flux (50wt% ethyline glycol and 50% glutamic acid hydrochloride) was added to the nanomaterial in order make a working solder joint.

Different samples were prepared by heating them at different temperatures and different times. Following the design of experiment described in the previous chapter, the following observations were made:

- Samples heated at 600°C did not produce a joint, independent of the time they were exposed to the temperature. As stated before, the solder would only melt completely at around 800°C.

- When heated for 20 seconds, the solder became burnt and the joint was lost. This is due to the oxidation of the copper.

The specimens prepared demonstrated good adherence of the nanomaterial on the copper. It was necessary to ensure that the solder was not heated too much such that the copper oxidizes or becomes burned. Too little time of heating however would mean adherence might not be achieved.

Figure 4.17: Fracture Surface of Testing Specimens.

49

For the tests, displacement speed was set at 1.5 mm/min. The specimens were the two copper strips soldered with the copper solder as explained previously. Each strip measures 45mm x 13mm. The figure below shows a schematic of the solder-strips assembly and parameters for the shear test. For this research, unless otherwise stated, *l = 40 mm, b = 5 mm* and *t = 0.25 mm.*
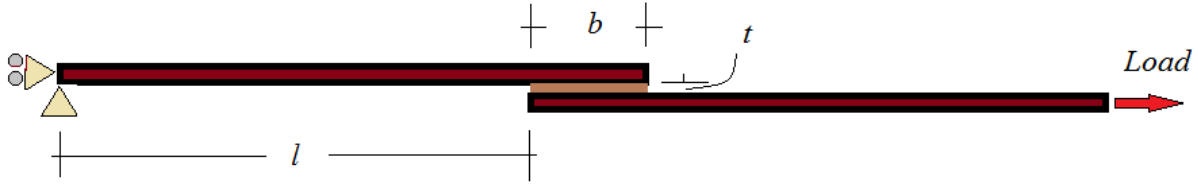

Figure 4.18: Schematic of solder-assembly for shear testing.

The average shear stress in the solder can be taken as the applied axial load divided by the solder joint area in contact with the copper strips. As for the shear strain, the common practice is to use the applied displacement divided by the solder thickness,

$$\tau = \frac{P}{A} \tag{4.1}$$

$$\gamma = \frac{\Delta l}{t} \tag{4.2}$$

Given the complex deformation fields involved in such type of loading, it is apparent that the shear strain calculation can only be considered as a rough estimate [44].

The first samples made were using the membrane as a whole as the solder. These membrane solders failed at loads ranging from 6 to 10 N. The figure below shows data of a specimen tested that failed under a 7.5 N load after a 0.36 mm displacement.
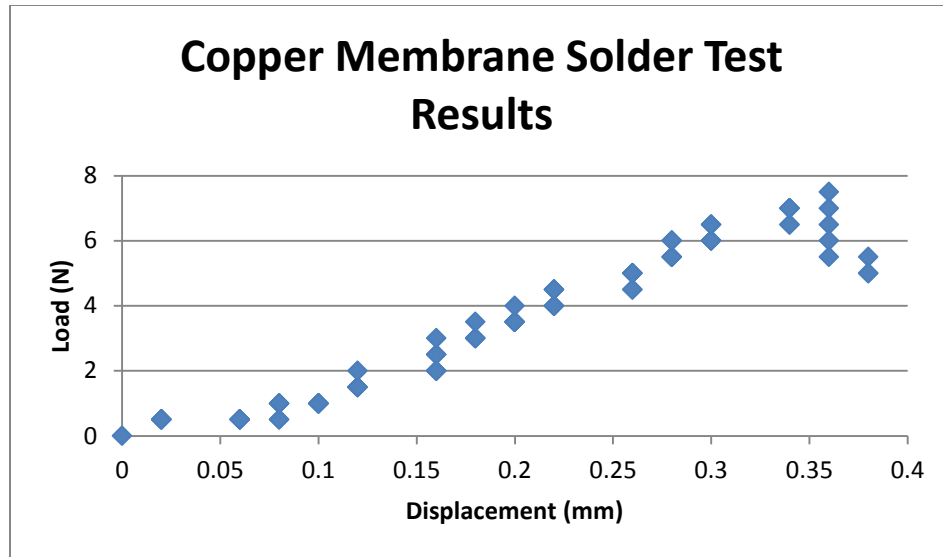
Figure 4.19: Membrane solder test results.

In order to improve the strength of the solder, creating a paste like solder was considered. In order to do so, membranes were cut up as finely as possible and mixed with the flux. The result is a paste solder as shown in the figure below.
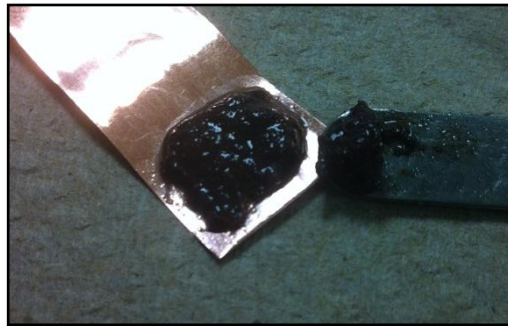
Figure 4.20: Copper solder paste.

As seen in Figure 4.15, the results obtained from the mechanical testing show considerable strength improvement of the solder when used as a paste. Specimens prepared with this method failed at loads ranging from 50 to 60 N at displacements of around 0.82 mm.

51

Figure 4.21: Paste solder test results.

A second set of test were performed to see the effect of lowering the solder thickness from 0.25 mm to 0.15 mm. Results can be seen in the figure below, showing loss of strength in the joint.
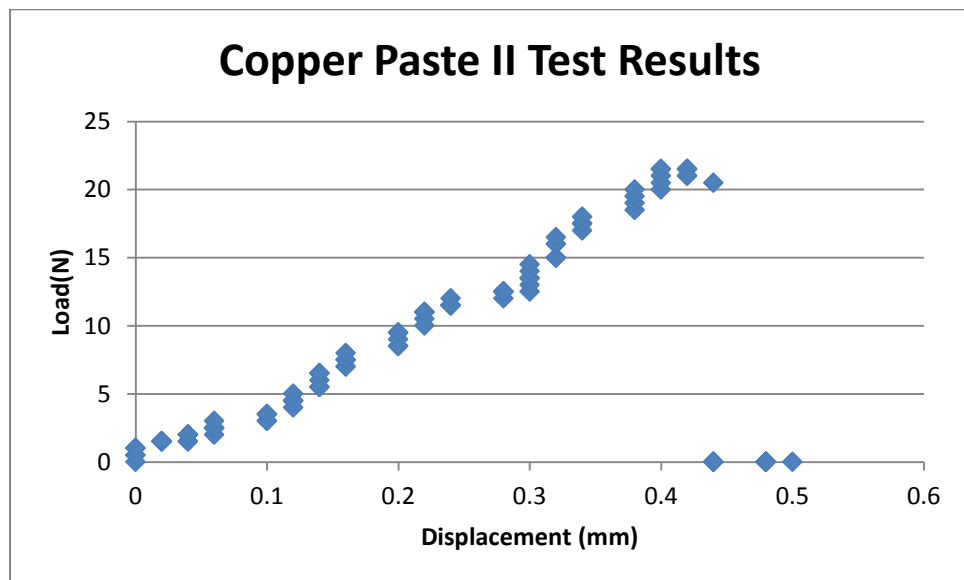
Figure 4.22: Paste solder test results with lower solder thickness.
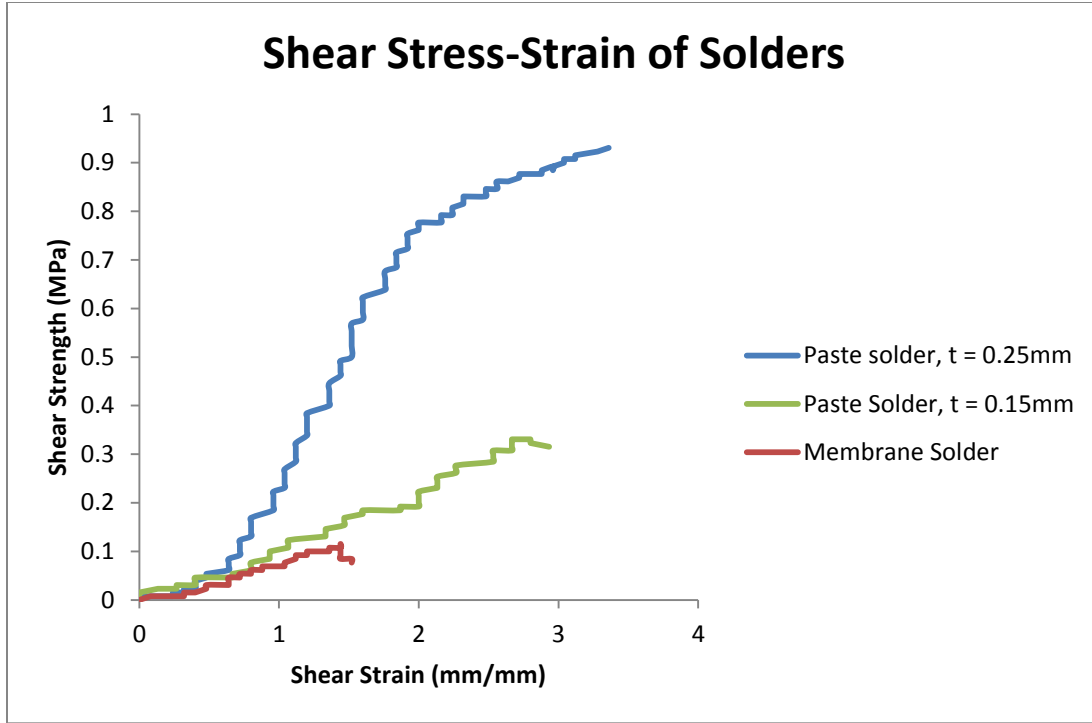
Figure 4.23: Shear Stress-Strain of Solders

Comparing the three cases studied, the following conclusions can be made:

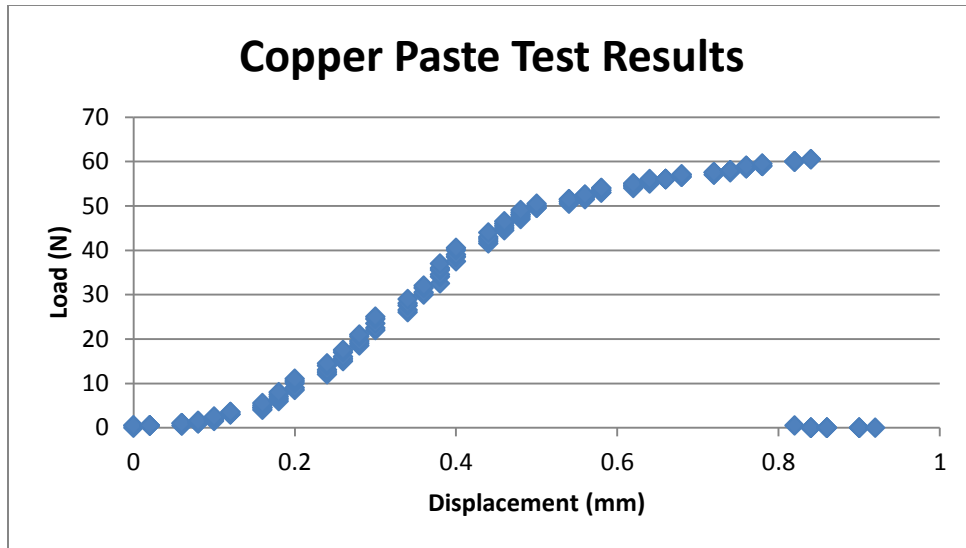- When it comes to the morphology of the solder, it is preferable to use a paste solder rather than the membrane alone if higher mechanical strength is desired.

- Solder thickness affects the strength of the joint: increased thicknesses causes greater deformation and higher shear strength.

To verify that the deformation of the copper strips does not affect the results, the deformation is calculated using the dimensions of the strips and the maximum force (60 N):

$$\delta = \frac{PL}{AE} = \frac{(60\ N) * (80mm)}{(0.25mm * 13mm) * (128GPa)} = 0.0115mm$$

Comparing with the deflection registered at this instant (0.82mm), only 1.4% of the load is used in the deflection of the copper strips.

In order to determine whether the copper nano-solder has any usability in real applications, the shear strength solder joints must support during thermal cycling will be calculated and compared with the results of the mechanical tests. A good sign of module to circuit board attachment is the survival of 1000 thermal test cycles between -55°C and 125°C as per specification MIL STD 883. Assume a scenario like the one pictured in the figure below:
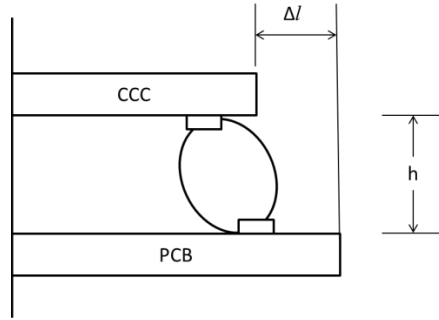
Figure 4.24: Surface Mount Deformation

Given the coefficients of thermal expansion of a ceramic module and an epoxy glass card and a 0.25 mm (*h*) high solder joint at a 10 mm (*r*) distance from the module center, the shear strain can be calculated as

$$\gamma = (\Delta\alpha)(\Delta T)\,r/h = (10 \times 10^{-6})(180)\,(10)/0.25 = 0.072 \tag{4.3}$$

Comparing with the results from the mechanical tests, the copper nano-solder can meet this demand, by withstanding up to 3 mm/mm shear strain. Furthermore, the shear force has been calculated under these conditions to be as follows [45]:

$$V \approx 0.01\,\Delta T\ (lbs) \tag{4.4}$$

Using the Δ(180°C) standard, the shear force results at around 8 Newtons. Resisting up to 60 Newtons, the copper nano-soder also meets this criteria.

CHAPTER 5: CONCLUSIONS AND FUTURE WORK

Nano-copper was successfully manufactured by electroless deposition on PAN nanofibers. Melting point and mechanical strength of the material was studied and tested. The following conclusions were drawn based on the obtained results:

- During the electroless plating process, careful monitoring of each step must be taken. Successful deposition of copper will occur only if the specimens are properly activated and the coating solution is maintained at a pH level of 11-12.

- Deposition of copper will mostly occur in the form of agglomerates. This is mostly due to initial nuclei undergoing rapid diffusion at the expense of the metal atoms in the solution. As more copper atoms are reduced in the solution, they tend to agglomerate around the initial nuclei.

- Copper deposition will occur both on the fibers and between them. This is due to palladium ions present between these spaces at the moment of the sample entering the coating stage. The palladium activates and nucleation begins, forming suspended agglomerates.

- With the described methodology, the effective thickness of the copper layer formed around the fibers ranges from 250 to 750 nm.

- The manufactured nano-copper had a melting range of 600-800°C. Copper deposited on top of the fibers melted at 600°C while interstitial copper, and thus the whole specimen,

melted at 800°C. This can be evidence of the template itself causing melting point depression on the nanomaterial.

- The lowered melting point confirms melting point depression occurs on copper, adding to the list of materials which present this property at the nanoscale..

- Flux is needed in order to create a solder bond with the produced nano-copper.

- Once bonding was achieved, mechanical testing could be performed. From the results, the solder could withstand loads ranging from 10-60N.

To help make the described nano-copper a better solder, a few steps can be taken in the future:

- Use smaller nanofibers as template to potentially make the particle size smaller and thus lower the melting point.

- Use better and more appropriate flux to better adhesion and increase strength.

Although in its current state the material is still far from being as viable as other lead-free alternatives, this research has demonstrated the potential of nanomaterials in lead-free technologies. The research has also contributed to the study of melting point depression of metals at the nanoscale and the potential applications of nanocopper in the electronics industry.

REFERENCES

[1]   Lead-free electronics. Ed. by Sanka Ganesan and Michael Pecht. Wiley-Interscience 2006

[2]   Dan Tao, Qufu Wei, Yibing Cai, Qiuxiang Xu and Lingyan Sun. "Functionalization of polyamide 6 nanofibers by electroless deposition of copper." 2008

[3]   J.M. Córdoba, M. Odén. "Growth and characterization of electroless deposited Cu films on carbon nanofibers." Surface & Coatings Technology 203 (2009) 3459–3464

[4]   M. Mikhaylova, M. Toprak, D. K. Kim, Y. Zhang, M. Muhammed. "Nanowire formation by electrodeposition in modified nanoporous polycrystalline anodic alumina templates." 2002.

[5]   H. Xing, L. Sun, G. Song, J. Gou and Y.W. Hao. Surface coating of carbon nanofibers/nanotubes by electrodeposition for multifunctionalization. 2008.

[6]   S. L. Lai, J. Y. Guo, V. Petrova, G. Ramanath, and L. H. Allen. "Size-Dependent Melting Properties of Small Tin Particles: Nanocalorimetric Measurements." Physical Review Letters. 1996.

[7]   Y.C. Sui, B.Z. Cui, R. Guardián, D.R. Acosta, L. Martínez, R. Perez. "Growth of carbon nanotubes and nanofibres in porous anodic alumina film." 2001.

[8]   Anthony Hart. "Materials World." Vol. 4 No. 5 pp. 265-67 May 1996.

[9]   Q. Chen. "Sol-gel nanocoating on commercial TiO2 nanopowder using ultrasound." SIMTech technical reports. Volume 11 Number 2 Apr-Jun 2010.

[10]   Electroless Plating: Fundamentals and Applications. Ed. by Glenn O. Mallory and Juan B. Hajdu. Noyes Publications/William Andrew Publishing. 1990.

[11]   Shoso Shingubara. "Fabrication of nanomaterials using porous alumina templates." Journal of Nanoparticle Research 5: 17–30, 2003.

[12]   Z. L. Xiao, Catherine Y. Han, U. Welp, H. H. Wang, W. K. Kwok, G. A. Willing, J. M. Hiller, R. E. Cook, D. J. Miller, and G. W. Crabtree. "Fabrication of Alumina Nanotubes and Nanowires by Etching Porous Alumina Templates." Nano Letters (2002)

[13]   Gokce Ugur, Mustafa M. Demir, Yuda Yurum, Yusuf Z. Menceloglu. "Metallized Carbon Nanofiber Fabrication For Fuel Cell Applications." Sabanci University, Faculty of Engineering and Natural Sciences.

[14]   K. Valenzuela, S. Raghavan, P. A. Deymier, and J. Hoying. "Formation of Copper Nanowires by Electroless Deposition Using Microtubules as Templates." Journal of Nanoscience and Nanotechnology. Vol. 8 1-6, 2008.

[15]   M. Zhang, M. Yu. Efremov, F. Schiettekatte, E. A. Olson, A. T. Kwan, S. L. Lai, T. Wisleder, J. E. Greene, and L. H. Allen. "Size-dependent melting point depression of

nanostructures: Nanocalorimetric measurements." Physical Review B. Volume 62, Number 15. (2000)

[16]   S. L. Lai, J. R. A. Carlsson, and L. H. Allen. "Melting point depression of Al clusters generated during the early stages of film growth: Nanocalorimetry measurements." Applied Physics Letters. Volume 72, Number 9. (1998)

[17]   M.E. Toimil, V. Buschmann, D. Dobrev, R. Neumann, R. Scholz, I.U. Schuchert and J. Vetter. "Single-Crystalline Copper Nanowires Produced by Electrochemical Deposition in Polymeric Ion Track Membranes." Advanced Materials 2001, 13, No.1.

[18]   S. Joo and D. F. Baldwin. "Performance of Silver Nano Particles as an Electronics Packaging Interconnects Material." Electronic Components and Technology Connference. 2007.

[19]   M.E. Toimil, J. Brötz, V. Buschmann, D. Dobrev, R. Neumann, R. Scholz, I.U. Schuchert and J. Vetter. "Ëtched heavy ion tracks in polycarbonate as template for copper nanowires." Nuclear Instruments and Methods in Physics Research. 2001. 192-197.

[20]   M.E. Toimil, E.M Höhberger, Chh. Schaeflein, R.H. Blick, R. Neumann, and C. Trautmann. "Electrical characterization of electrochemically grown single copper nanowires." Applied Physics Letters. 2003. Volume 82, Number 13.

[21]   H.W. Sheng, G. Ren, L.M. Peng, Z.Q. Hu and K. Lu. "Superheating and melting point depression of Pb nanoparticles embedded in Al matrices."Philosophical Magazine Letters. 1996. Volume 73, No. 4, 179-186.

[22]   R. Goswami and K. Chattopadhyay. "Depression of melting point of multidomained bismuth in aluminum based metallic glass nanocomposites." Center for Advanced studies, Department of Metallurgy, Indian Institute of Science.

[23]   Anton Zoran Miric and Angela Grusd. "Lead-free alloys." Soldering and Surface Mount Technology. 10/1 [1998] 19-25.

[24]   E. Ferain and R. Legras. "Tempates for engineered nano-objects for use in microwave, electronic devices and biomedical sensing application." The Seventh International Symposium on Swift Heavy Ions in Matter. Version 2. 2008.

[25]   Chennapragada, Pavani, "Fabrication of palladium nanoparticles and nanoporous alumina templates" (2005). Theses and Dissertations. Paper 2821.

[26]   A. Bargang, L. Lrxiang and L. Hongxi. "Preparation of carbon nanotube composite material with metal matrix by electroplating." Trans. Nonferrous Met. Soc. China. Vol. 15 No. 5. 2005.

[27]   T. Gao, G. Meng, Y. Wang, S. Sun, L. Zhang. "Electrochemical synthesis of copper nanowires." Journal of Physics: Condensed Matter. 2002. 355-363.

[28]   H. Jiang, K. Moon, F. Hua and C.P. Wong. "Thermal Properties of Tin/Silver Alloy Nanoparticles for Low Temperature Lead-free Interconnect Technology." Electronic Components and Technology Conference. 2007.

[29]   X.W. Wang, G.T. Fei, K. Zheng, Z. Jin and L.D. Zhang. "Size-dependent melting behavior of Zn nanowire arrays." Applied Physics Letters 88. 2006.

[30]   K. Mohan Kumar, V. Kripesh and Andrew A.O. Tay. "Sn-Ag-Cu Lead-free Composite Solders for Ultra-Fine-Pitch Wafer-Level Packaging." Electronic Components and Technology Conference. 2006.

[31]   S.M.L. Nai, J. Wei and M. Gupta. "Multi-walled carbon nanotubes reinforced lead-free solder composites." SIMTech technical reports. Volume 9, No. 4. 2008.

[32]   L. Y. Hsiao and J. G. Duh. "Synthesis and characterization of lead-free solders with Sn-3.5Ag-xCu (x=0.2, 0.5, 1.0) alloy nanoparticles by the chemical reduction method." Journal of the Electrochemical Society, 152. 2005.

[33]   J. Oh, Y. Tak and J. Lee. "Electrodeposition of Cu_2O Nanowires Using Nanoporous Alumina Template." Electrochemical and Solid-State Letters, 7. 2004.

[34]   K. Nielsch, F. Miller, A. Li and U. Gösele. "Uniform Nickel Deposition into Ordered Alumina Pores by Pulsed Electrodeposition." Advanced Materials, 12, No. 8. 2000.

[35]   S. Shulkla, S. Seal, Z. Rahaman and K. Scammon. "Electroless copper coating of cenospheres using silver nitrate activator." Materials Letters 57 (2002) 151-156.

[36]   J. Lim, J. Moon, G. Yi, C. Heo and S. Yang. "Fabrication of One-Dimensional Colloidal Assemblies from Electrospun Nanofibers." Langmuir Volume 22, No. 8. 2006.

[37]   A. Buldum, C.B. Clemons, E.A. Evans, K. Kreider and G.W. Young. "Coating Growth on Nanofibers: Multi-Scale Modeling, Simulations and Experiments."NSTI-Nanotech 2004. Vol. 3.

[38]   J. Sun and S.L. Simon. "The melting behavior of aluminum nanoparticles." Thermochimica Acta 463 (2007) 32-40.

[39]   H.W. Sheng, G. Ren, L.M. Peng, Z.Q. Hu and K. Lu. "Epitaxial dependence of the melting behavior of In nanoparticles embedded in Al matrices." Journal of Materials Research. Volume 12, No. 1. 1997.

[40]   K. Chattapadhyay and R. Goswami. "Melting and superheating of metals and alloys." Progress in Materials Science. Vol. 42, pp. 287-300, 1997.

[41]   H. W. Sheng, K. Lu and E. Ma. "Melting and freezing behavior of embedded nanoparticles in ball-milled Al-10wt% M (M = In, Sn, Bi, Cd, Pb) mixtures." Acta Mater, Vol. 46, No. 14, pp. 5195-5205. 1998.

[42]   Y. Shibuta and T. Suzuki. "Melting and nucleation of iron nanoparticles: A molecular dynamics study." Chemical Physics Letters 445 (2007) 265-270.

[43]   K. Lu and Z.H. Jin. "Melting and superheating of low-dimensional materials."Current Opinion in Solid State and Materials Science 5 (2001) 39-44.

[44]   Y.L. Shen, N Chawla, E.S. Ege and X. Deng. "Deformation Analysis of lap-shear testing of solder joints." Acta Materiala 53 (2005) 2633-2642.

[45]   Peter A. Engel. "Structural Analysis of Printed Circuit Board Systems." Springler-Verlag New York, Inc. 1993.